Haloing in bimodal magnetic colloids: The role of field-induced phase separation

C. Magnet,[1] P. Kuzhir,[1] G. Bossis,[1] A. Meunier,[1] L. Suloeva,[2] and A. Zubarev[3]

[1]*University of Nice Sophia Antipolis, Laboratory of Condensed Matter Physics, CNRS UMR 7663, Parc Valrose, 06108 Nice Cedex 2, France*

[2]*Belarussian National Technical University, 65, Prospekt Nezavisimosti, Minsk 220013, Belarus*

[3]*Department of Mathematical Physics, Ural State University, 51, Prospekt Lenina, Ekaterinburg 620083, Russia*

(Received 8 April 2012; revised manuscript received 20 June 2012; published 13 July 2012)

If a suspension of magnetic micrometer-sized and nanosized particles is subjected to a homogeneous magnetic field, the nanoparticles are attracted to the microparticles and form thick anisotropic halos (clouds) around them. Such clouds can hinder the approach of microparticles and result in effective repulsion between them [M. T. López-López, A. Yu. Zubarev, and G. Bossis, Soft Matter **6**, 4346 (2010)]. In this paper, we present detailed experimental and theoretical studies of nanoparticle concentration profiles and of the equilibrium shapes of nanoparticle clouds around a single magnetized microsphere, taking into account interactions between nanoparticles. We show that at a strong enough magnetic field, the ensemble of nanoparticles experiences a gas-liquid phase transition such that a dense liquid phase is condensed around the magnetic poles of a microsphere while a dilute gas phase occupies the rest of the suspension volume. Nanoparticle accumulation around a microsphere is governed by two dimensionless parameters—the initial nanoparticle concentration (ϕ_0) and the magnetic-to-thermal energy ratio (α)—and the three accumulation regimes are mapped onto a α-ϕ_0 phase diagram. Our local thermodynamic equilibrium approach gives a semiquantitative agreement with the experiments on the equilibrium shapes of nanoparticle clouds. The results of this work could be useful for the development of the bimodal magnetorheological fluids and of the magnetic separation technologies used in bioanalysis and water purification systems.

DOI: 10.1103/PhysRevE.86.011404 PACS number(s): 83.80.Hj, 47.65.Cb, 64.75.Xc

I. INTRODUCTION

Bimodal colloidal mixtures of nanoparticles and microparticles may show different phase behaviors depending on the interparticle interactions and on the volume fractions of both species. If the nanoparticles bear a relatively strong electric charge and the microparticles are weakly charged, then the suspension experiences a phase transition from a colloidal gel to a stable fluid and back to a colloidal gel with increasing nanoparticle concentration [1]. The stabilization of such a binary mixture was attributed to the formation of thin shells (halos) with a high local nanoparticle concentration around the microparticles; such a stabilization phenomenon is being referred to as haloing. Monte Carlo simulations and theoretical studies based on integral equations have shown that the haloing effect appears as a result of the interplay between a strong electrostatic repulsion between nanoparticles and a weak colloidal attraction of nanoparticles to large microparticles [2–5].

In the above cited studies the haloing phenomenon was governed by the competition between electrostatic and van der Waals interactions. Any additional interaction between microparticles and nanoparticles is expected to strongly affect the phase behavior of the mixture, especially if this interaction is long ranged. This is the case of bimodal suspensions composed of magnetizable microparticles and nanoparticles, whose colloidal stability has been studied in Refs. [6,7]. The addition of a few volume percent of magnetite nanoparticles to the initial suspension of carbonyl iron microspheres has been found to avoid aggregation of microspheres under van der Waals forces and, consequently, to considerably decrease their sedimentation. At the same time, nanoparticle clouds of a thickness of the order of $0.1D$ were observed around the microspheres (here D is the microsphere diameter). The halo appearance was qualitatively explained by the competition between steric repulsion between oleate-coated nanoparticles and weak magnetic attraction between the microsphere and the surrounding nanoparticles, which occurs due to the remnant magnetization of the former. In the presence of an external magnetic field, the microspheres get magnetized and attract each other, forming field aligned structures, while the presence of magnetic nanoparticles can either enhance or weaken the mechanical properties of the mixture depending on the nanoparticle size. In the case of relatively small nanoparticles (with a diameter $d<10$ nm), the magnetic attractive force between two microspheres is enhanced by a factor equal approximately to the magnetic permeability of the nanoparticle phase of the bimodal suspension [8]. In the case of larger nanoparticles ($d>15$ nm), nanoparticle-nanoparticle and nanoparticle-microsphere interactions become strong enough to induce a significant migration of nanoparticles towards the microspheres, resulting in thick nanoparticle clouds that hinder the approach of the two microspheres and create an effective repulsion between them [9]. Clearly, if the addition of nanoparticles leads to a strong increase in the intersphere gap, the force required to separate two microspheres could be significantly reduced, which will lead to a decrease of the magnetorheological effect of the suspension. Therefore, a deep understanding of the effects of nanoparticle size and volume fraction is crucial for the development of magnetorheological fluids based on bimodal magnetic suspensions.

For a better understanding of this phenomenon, a more detailed investigation of the field-induced halo formation around a single microsphere is highly desirable. This problem approaches the well-studied phenomena of the diffusion and accumulation of magnetic nanoparticles around either a magnetized wire or a spherical magnetic microparticle, both modeling the collector unit of high gradient magnetic

separators. These devices are being extensively used in the ore beneficiation industry [10], in the separation of magnetically labeled biological molecules or cells [11], as well as in recent laboratory experiments on magnetically assisted water purification systems [12]. The existing theoretical studies were mostly carried out under an approximation of noninteracting magnetic nanoparticles. They report concentration profiles of the magnetic nanoparticles [13,14], as well as the size and shape of the nanoparticle cloud (region with a high particle volume fraction) around a magnetized wire [15–17]. According to these theories, the static equilibrium concentration profiles follow the Boltzmann statistical distribution while the nanoparticle static cloud around a magnetized collector is simply considered as a region where the particle volume fraction (given by the Boltzmann distribution) exceeds the maximum packing fraction of about 0.6. Clearly, the approximation of noninteracting nanoparticles is irrelevant for predictions of the shape and the size of closely packed particle buildups. Furthermore, even at the initial stage of the particle capture without any buildup around the collector, the nanoparticles of a size as small as 15–20 nm may already exhibit a rather strong attraction between them and even show a condensation phase transition above some critical magnetic field and volume fraction [18–20]. A few attempts have been made to take into account the interactions between nanoparticles in magnetic separation systems [15,21,22]. However, they seem to be very approximate, and the effect of interparticle interactions on the nanoparticle capture efficiency was poorly analyzed. A rigorous equilibrium thermodynamic approach needs to be employed for these systems, and, consequently, eventual phase transitions need to be considered. Furthermore, only a few visualization experiments on nanoparticle accumulation around a magnetized wire have been reported [23,24]. These studies are restricted to some limited sets of experimental parameters (external magnetic field, nanoparticle size, elapsed time) and do not allow a quantitative comparison with the theories.

In the present paper, we report a systematic experimental and theoretical study of the magnetic nanoparticle accumulation around a single magnetic microsphere in the presence of an external magnetic field. The experimental part focuses on the effect of the nanoparticle size (d), the initial volume fraction (ϕ_0), and the external magnetic field (H_0) on the redistribution of nanoparticle concentration and, particularly, on the size and shape of the concentrated regions of nanoparticles—the so-called nanoparticle clouds—around a microsphere. As in the study of phase separation in magnetic colloids [18,25], the theoretical approach of these effects is based on the local thermodynamic equilibrium approach, in which the dipole-dipole and hard-sphere potentials acting between the nanoparticles are naturally introduced in the thermodynamic functions of the magnetic nanoparticle suspension. The constitutive equations of state of the nanoparticle suspension (osmotic pressure and chemical potential as a function of the nanoparticle concentration) are formulated. The gas-liquid phase transition in the nanoparticle suspension is then studied and the binodal curves separating different phases are calculated. The particle concentration profile around a microsphere is found from the condition of the uniformity of the chemical potential of nanoparticles across the suspension, taking into account the eventual phase transitions. The nanoparticle clouds are expected to correspond to regions of the condensed liquid state of the ensemble of nanoparticles around a microsphere, rather than to regions of closely packed nanoparticles, as follows from the existing theories. The present theory and experiments will allow us to establish an important fundamental and practical result: We shall find the threshold parameters (d,ϕ_0,H_0), above which the thermodynamic equilibrium between the nanoparticle liquid phase (nanoparticle cloud) and gas phase (the rest of the nanoparticle suspension) is not possible anymore, meaning that the clouds grow infinitely, adsorbing all the surrounding nanoparticles. This study is motivated by practical applications in both magnetorheological smart technologies and magnetic separation techniques.

The present paper is organized as follows. In Sec. II, we shall describe the experimental setup and characterize the synthesized nanoparticle suspensions. Section III will be devoted to the experimental results on the visualization of the accumulation of nanoparticles around a microsphere. In Sec. IV, we shall present the local thermodynamic equilibrium approach and calculate the concentration profiles and the shape and size of the nanoparticle clouds. In the same section we shall compare our theory to experimental results. In Sec. V, the concluding remarks will be outlined and perspectives for further investigations will be discussed.

II. EXPERIMENT

A. Experimental setup

The experimental cell used for the visualization of the redistribution of the magnetic nanoparticle concentration around a magnetized microsphere is shown schematically in Fig. 1. First, a bimodal aqueous suspension of magnetite nanoparticles and nickel microspheres was prepared by a dilution of a primary concentrated ferrofluid up to a desired nanoparticle volume fraction (ranging from $\phi_0 = 0.005\%$ to 0.16%) with the subsequent addition of an extremely small quantity of nickel micropowder. Nickel microparticles possessed a well-defined spherical shape and a narrow size distribution with a mean diameter of $D \approx 5\ \mu$m. Magnetite

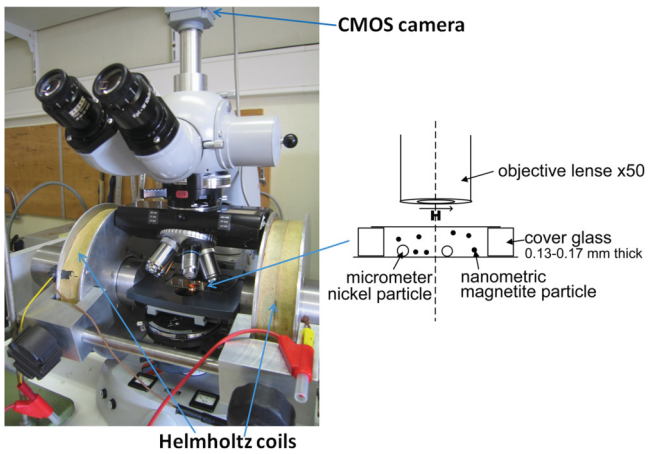

FIG. 1. (Color online) Experimental cell used for visualization of nanoparticle accumulation around microspheres.

TABLE I. Properties of the primary ferrofluids and particle size characteristics.

Sample	Density, ρ (g/cm^3)	Particle volume fraction ϕ (%)	Saturation magnetization M_s(kA/m)	Initial magnetic susceptibility χ	Particle size by TEM	Particle (cluster) size by DLS		
					Volume mean diameter d_{43}(nm)	Volume mean diameter (nm)	z-average diameter (nm)	Polydispersity index
(I)	1.045	1.07	4.38	0.077	11	18	25	0.27
(S)	1.175	4.2	21.9	0.78	13	62	82	0.20

nanoparticles (or rather aqueous ferrofluids) were synthesized by two different methods described in Sec. II B. A drop of the bimodal suspension was then sandwiched between two glass plates separated by a gap of 0.13–0.17 mm. This fixture was then placed under a transmitted light optical microscope (Carl Zeiss Photomicroscope III) equipped with a camera PixelInk PL-B742U equipped with a complementary metal oxide semiconductor (CMOS) color image sensor. An external magnetic field, parallel to the glass plates, of an intensity ranging from $H_0 = 0$ to 16 kA/m, was generated by a pair of Helmholtz coils placed around the microscope. Iron yokes were introduced into Helmholtz coils in order to reinforce the magnetic field. Nevertheless, measurements showed that the magnetic field was homogeneous, within a few percent tolerance, in the location of the bimodal suspension drop. Therefore, nickel microspheres did not migrate towards one or another coil during 3 h of experiments. A 50-fold objective (Olympus LMPlanFl 50×0.50) was used for observation of the suspension. Once the magnetic field was applied, nickel microspheres were magnetized and the magnetite nanoparticles started to migrate towards the microspheres such that their volume fraction increased in the vicinity of the magnetic poles of microspheres forming clouds extended along the direction of the external magnetic field. Such a redistribution of nanoparticle concentration was detected by the change in contrast of the suspension. Pictures of the observed microsphere with its nanoparticle clouds were taken every 30 s for 30 min, starting from the moment when the magnetic field was applied. The sequence of pictures was then analyzed using IMAGEJ software to extract the geometrical parameters of the nanoparticle clouds (longitudinal size). In some experiments, the formation of nanoparticle clouds was a relatively long process and the duration of the observation was increased up to 3 h. To avoid water evaporation from the nanoparticle suspension during long-time experiments, between two glass plates we sandwiched a ring pattern of a mixture of poly(methyl methacrylate) (PMMA) microbeads (Microbeads Spheromers ®CA) with acyanocrylate glue and introduced a drop of the magnetic suspension with the help of a microneedle inside the so-formed ring seal. In these specific experiments, the monodisperse PMMA beads of diameter 31 μm served as well-calibrated separators between the two glass plates. The quantity of nickel microspheres in the suspension was small enough such that they were sufficiently spaced from each other, their dipolar interactions were weak enough, and they did not attract each other. The nanoparticle clouds of neighboring microspheres did not interact with each other, so the experimental conditions were close to the case considered in our theory—a single microsphere placed in an infinite volume of a nanoparticle suspension.

B. Nanoparticle synthesis and characterization

We used two kinds of magnetite in water solutions (ferrofluids) with different nanoparticle sizes. Both samples were prepared by a coprecipitation of ferrous and ferric salts in an alkali medium [26]. Magnetite nanoparticles were subsequently stabilized by either electrostatic (ionic [27]) or entropic (steric double layer [28]) repulsion; these two samples are hereinafter denoted by (I) and (S), respectively.

Both kinds of magnetite nanoparticles and their aqueous solutions were characterized by transmission electron microscopy (TEM, JEOL JEM 1400), dynamic light scattering (DLS, Malvern ZetaSizer Nano ZS), pH measurements (Mettler Toledo GmBH Seven Easy pH), conductivity and ζ-potential measurements (Malvern ZetaSizer Nano ZS), and vibrating sample magnetometry (VSM 4500 EG&G Princeton Applied Research). Some physical properties of both primary ferrofluids are summarized in Table I.

The TEM pictures of both samples are shown in Fig. 2 and the corresponding nanoparticle size distribution is shown in Fig. 3(a). Both samples (I) and (S) have a size distribution extended from 4 to about 20 nm with volume mean diameters d_{43}^{TEM} equal to 11 and 13 nm, respectively. The nanoparticles of the sample (I) seem to be weakly aggregated while those of the sample (S) are gathered in irregularly shaped clusters with a mean size estimated to be of the order of 50–70 nm. Such an aggregation of oleic-acid stabilized nanoparticles has already been reported in Ref. [28] but its cause remains unexplained. The appearance of the clusters in the sterically stabilized ferrofluid (S) did not affect its sedimentation stability for at least half a year but improved considerably their capture

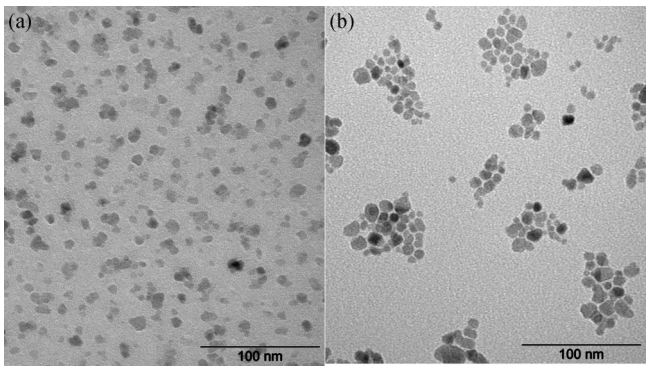

FIG. 2. TEM images of the two ferrofluid samples: (a) ionic stabilization; (b) steric stabilization with a double-layer oleic surfactant.

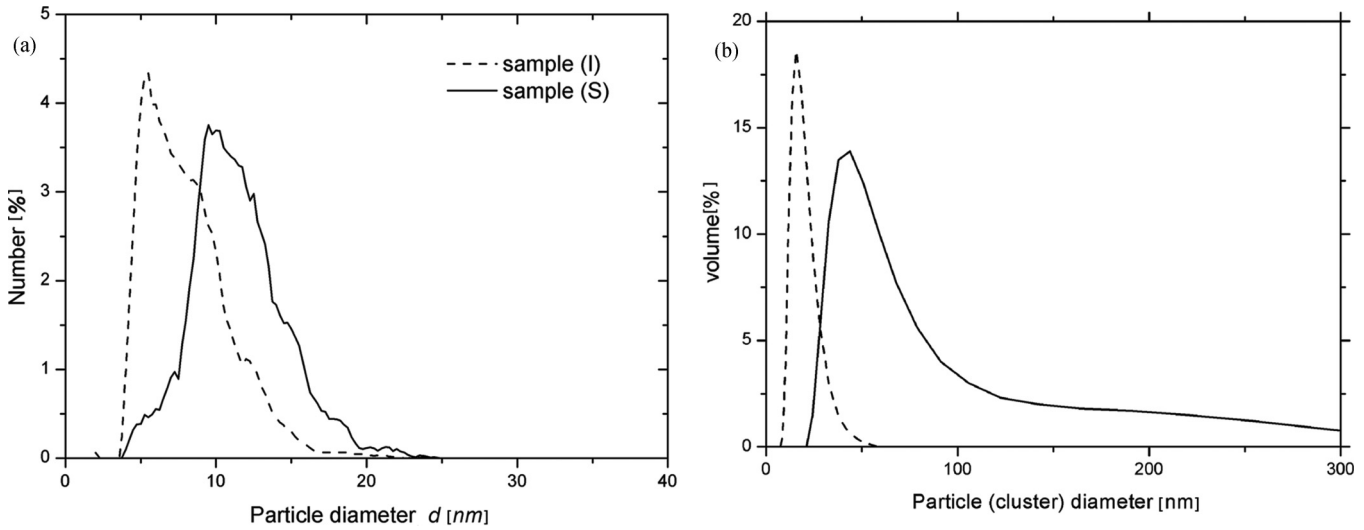

FIG. 3. Nanoparticle size distribution obtained from transmission electron microscopy (a) and dynamic light scattering (b): The dashed line is the ferrofluid sample (I), and the continuous line is the ferrofluid sample (S).

efficiency compared to that of quasi-isolated nanoparticles of the ferrofluid (I). The particle size distribution obtained by DLS (for diluted ferrofluids at a particle volume fraction $\phi = 0.005\%$) is shown in Fig. 3(b) and the volume mean diameter for sample (I), $d^{\mathrm{DLS}} = 18$ nm, appears to be about 1.6 times the one obtained from TEM pictures. This corroborates a weak particle aggregation revealed by TEM [Fig. 2(a)]. The sample (S) shows a much more pronounced difference between the TEM and the DLS size distributions: The DLS volume mean diameter, $d^{\mathrm{DLS}} = 62$ nm, appears to be about five times the TEM diameter and corresponds approximately to the mean size of the nanoparticle clusters observed by TEM.

The results of the measurements of the particle ζ potential and of the electric conductivity of (I)- and (S)-type dilute suspensions are summarized in Table II for particle volume fractions $\phi = 0.005\%$ and $\phi = 1.6\%$, covering the concentration range used in the visualization experiments. As expected, the (I) samples have an acidic pH, and their nanoparticles bear a positive electric charge characterized by a relatively high ζ potential, $\zeta \sim +50$ mV, which is approximately the same within the particle concentration range considered. On the contrary, the conductivity and, consequently, the ionic strength of (I)-type suspensions decreases six times with a decrease in particle concentration from $\phi = 0.16\%$ to $\phi = 0.005\%$. This can be explained by a decrease of concentrations of H^3O^+ and Fe^{3+} ions when the nanoparticle suspension is progressively diluted. In any event, the suspension ionic strength is low enough ($I < 20$ mM) to avoid a significant screening of electric charges on the particle surface. Using the classical Derjaguin-Landau-Verwey-Overbeek (DLVO) theory [29] completed with magnetic dipolar interactions, we have estimated the potential energy of the resultant interaction between the two particles in the case when their magnetic moments are aligned along the line connecting the particle centers. The value $U_{\max} \sim 4kT$ of the potential barrier does not seem to be high enough to provide long-time stability of the suspension, even though the secondary minimum of the potential energy appears to be quite small: $U_{\min} \sim -0.5kT$. This likely corroborates the weak aggregation state revealed by TEM and DLS measurements. However, the sedimentation tests show that, in the considered concentration range, the (I) suspensions remain stable for at least half a year.

On the other hand, the stability of the relatively large nanoclusters of the (S)-type suspensions is not evident. The oleic-based surfactant double layer as thin as 1 or 1.5 nm [31,32] cannot by itself avoid aggregation, as follows from the

TABLE II. Electrostatic properties of the nanoparticles/nanoclusters surface.

Suspension	Particle volume fraction $\phi(\%)$	Suspension pH	Suspension electric conductivity σ (μSm/cm)	ζ potential (mV)	Ionic strength I (mM)	Debye length κ^{-1} (nm)	Potential barrier[a] $U_{\max}/kT$
(I)	0.005	4.0	170	+47	2.6	6.1	8.3(4.5)[b]
(I)	0.16	3.1	990	+49	15	2.5	7.4(4.1)[b]
(S)	0.005	8.3	280	−59	4.2	4.8	83[c]
(S)	0.16	9.5	450	−57	6.8	3.8	72[c]

[a]The potential energy versus interparticle separation was estimated with the help of the DLVO theory [29] using the linear superposition approximation for the electrostatic interaction (with the ζ-potential values used for the surface potential ψ_0) and the classical Hamaker approximation (with the nonretarded Hamaker constant for the magnetite-water system $A_H \approx 33 \times 10^{-21}$ J [30]).

[b]The mean diameter of isolated nanoparticles was taken from TEM measurements: $d = 11$ nm. The values in parentheses are estimated taking into account the magnetic interactions between nanoparticles with magnetic moments aligned along the line connecting the particle centers.

[c]The mean diameter of nanoclusters was taken from DLS measurements: $d = 62$ nm. Estimations are done for zero magnetic field.

estimation of the van der Waals interaction potential between two nanoclusters of a mean diameter $d = 62$ nm at a separation equal to 2–3 nm. Hopefully, the clusters with their double layers bear a relatively high negative charge corresponding to a ζ potential of about -60 mV. The conductivity and the ionic strength of the both tested (S) suspensions are relatively low ($I < 10$ mM), so the electrostatic repulsion is again favored, providing a potential barrier in the absence of the magnetic field of about $U_{\max} \sim 70\,kT$ and a negligible secondary minimum of $U_{\min} \sim -0.01kT$. In the presence of the magnetic field, nanoclusters get magnetized and their dipolar attraction lowers substantially the potential barrier level, and a pronounced secondary minimum appears. For instance, at a magnetic field $H = 48$ kA/m (as the one in the vicinity of the magnetic microspheres in our experiments), the resultant interaction between two nanoclusters is strongly attractive (with $U_{\min} \sim -50\,kT$) at any interparticle separation that is larger than the thickness of the surfactant double layer. This corresponds to a strong field-induced aggregation of nanoclusters observed in experiments at magnetic fields $H > 10$ kA/m. However, the reversible character of this aggregation proves the efficiency of the surfactant double layer: At high magnetic fields, the electrostatic repulsion is not strong enough to separate the nanoclusters but the surfactant layer avoids close contact between them; when the magnetic field is switched off, the overlapping electric double layers of nanoclusters repel each other and reestablish the initial dispersion state of the suspension, which does not lose its sedimentation stability after switching off of the magnetic field. Such a combined steric-electrostatic mechanism of the stabilization of aqueous solutions of magnetite nanoparticles covered with an oleate double layer has been reported in Ref. [33], where it was shown that the absolute value of the nanoparticle ζ potential increased gradually with the growth of sodium oleate adsorbed on the particle surface and became quasi-insensitive to the suspension pH, providing good colloidal stability in a wide pH range.

Magnetization $M(H)$ curves of both primary concentrated ferrofluids are shown in Fig. 4, with H being the magnetic field intensity and M the magnetization. The time steps of the measurements were sufficiently long to ensure an equilibrium structure of the ferrofluid at each imposed magnetic field intensity H. The magnetization saturation M_S of the ferrofluids (see Table I) was found by an extrapolation of the M vs $1/H$ dependencies to zero value of $1/H$ in a range of high values $H/M \gg 1$ [26]. The magnetization of the nanoparticles was simply estimated as the ratio of ferrofluid saturation magnetization to the particle volume fraction ϕ of ferrofluids, $M_p = M_S/\phi$, and was found to be close to the saturation magnetization of bulk magnetite (480–520 kA/m) for both samples. The shape of the $M(H)$ curves was essentially similar for both ferrofluids (I) and (S) without a distinguishable hysteresis. Nevertheless, the magnetization mechanism is expected to be rather different because the (S) sample experienced a reversible phase separation under applied magnetic field, while the (I) sample did not, as follows from optical microscopy. A relatively dilute (I) sample ($\phi = 1.07\%$) composed of quasi-isolated superparamagnetic particles should presumably follow the Langevin magnetization law [26] $M = M_S[\coth(\mu_0 m H/kT) - kT/(\mu_0 m H)]$, where $\mu_0 = 4\pi \times 10^{-7}$ H/m is the magnetic permeability of vacuum, $m = M_p V_p$ is the particle magnetic moment, $V_p = \pi d^3/6$ is the particle volume, d is the mean particle diameter, $k = 1.38 \times 10^{-23}$ J/K is the Boltzmann constant, and $T \approx 300$ K is the absolute temperature of the suspension. The mean particle size d of the sample (I) was estimated by fitting the experimental magnetization curve to the Langevin function, which gave a value of $d_{\text{magn}} \approx 9$ nm, which is close to the one obtained by TEM.

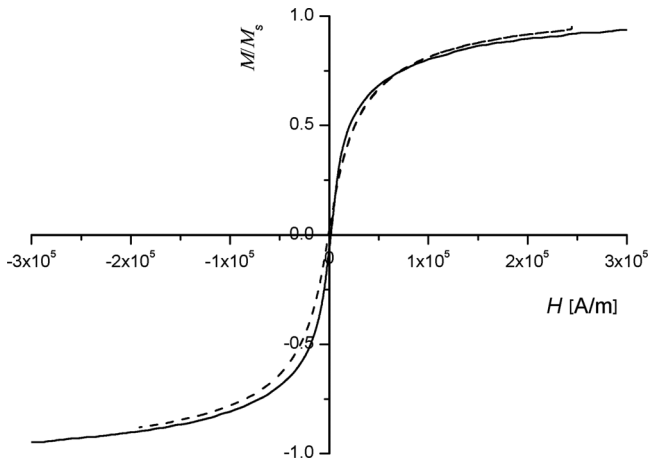

FIG. 4. Magnetization curve of both synthesized ferrofluids: The solid line corresponds to the sterically stabilized (S) sample and the dashed line to the ionically stabilized (I) sample.

The (S) sample was composed of nanoparticle clusters of a mean diameter of 60–70 nm. Each individual cluster contains a few dozen closely spaced nanoparticles at an internal volume fraction of the order of $\phi_{\text{int}} \sim 0.5$, as estimated from TEM pictures. Clearly, in the presence of an external field, the magnetization of these clusters should be strongly affected by many-body interactions between fluctuating magnetic dipoles of each superparamagnetic nanoparticle. Therefore, we expect a strong deviation of the nanocluster magnetization from the Langevin law. Furthermore, upon application of a strong enough magnetic field, the nanoclusters are assembled into long columns aligned with the field lines. Thus, the ferrofluid magnetization will depend, among other things, on its internal structure. Searching for a theoretical magnetization law for the clustered ferrofluid sample (S) becomes a difficult task. However, for the interpretation and the modeling of the nanocluster capture process, we do not need a precise form of the magnetization law of the primary ferrofluid but rather of the initial magnetic susceptibility χ_c of the nanoclusters. This magnitude is more easily estimated from measurements of the magnetization of a compacted dry extract of the primary ferrofluid. These measurements give a value of $\chi_c \approx 9$ for the nanocluster susceptibility.

III. OVERVIEW OF OBSERVATION RESULTS

Most of the visualization experiments were carried out with the (S)-ferrofluid sample because the nanoclusters of this sample were sufficiently large and experienced a rather strong interaction with microspheres—the most important case for practical applications. A sequence of pictures

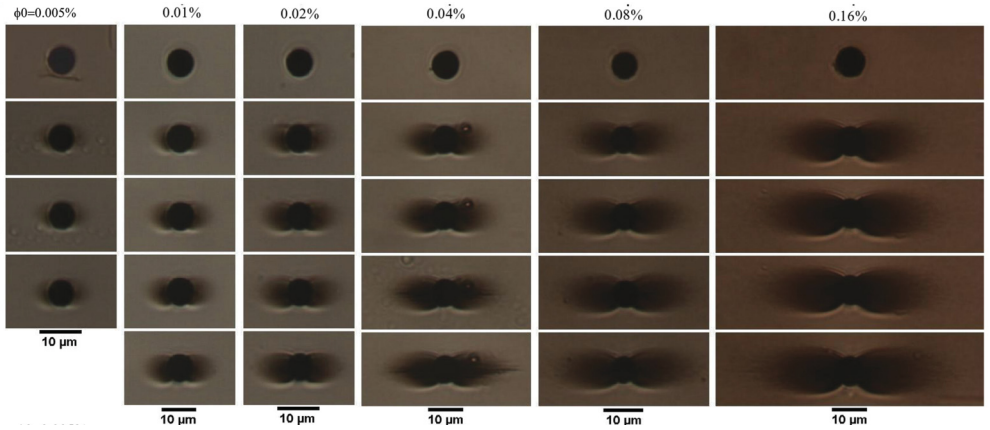

FIG. 5. (Color online) Influence of the initial volume fraction of nanoparticles ϕ_0 on the size of the nanoparticle clouds. The nanocluster concentration is related to the nanoparticle concentration through the relation $\Phi_0 = \phi_0/\phi_{\text{int}}$, with $\phi_{\text{int}} \approx 0.5$ being the internal volume fraction of nanoclusters. The magnetic field intensity is $H_0 = 16$ kA/m; the image sequence from the top to the bottom corresponds to different elapsed times: 0, 5, 10, 15, and 20 min.

illustrating the nanocluster accumulation around a magnetic microsphere is shown in Fig. 5 for an external magnetic field of $H_0 = 16$ kA/m, for different initial concentrations of the nanoparticles ϕ_0 and for different times after the onset of the magnetic field. As we see in these pictures, the nanoparticle clouds have a lobe shape and show an axial symmetry with respect to the microsphere axis that is parallel to the external magnetic field. Such anisotropy of the nanoparticle clouds comes from the anisotropy of magnetic interactions between the nanoclusters and the microsphere: This interaction is attractive within the regions where the magnetic field H is higher than the external field H_0 while it is repulsive in the regions where $H < H_0$. The attractive regions are therefore formed in the vicinity of the two magnetic poles of the microsphere and the repulsive region is adjacent to the microsphere equator, where magnetite nanoclusters never accumulate. Figure 5 also shows that the volume of the nanoparticle clouds increases both with elapsed time and with an initial concentration of the nanoparticles ϕ_0 in the suspension. The latter effect is explained by stronger dipolar interactions between the nanoclusters in a more concentrated suspension. This enhances their response to the applied magnetic field and ensures a stronger attraction to the magnetic microsphere. The transmitted light intensity and, consequently, the nanoparticle concentration inside the clouds seem to increase considerably with ϕ_0: At concentrations $\phi_0 \geqslant 0.04\%$, a large part of the cloud becomes opaque, which makes it impossible to measure the concentration profiles by means of image processing. As we shall see in the next section, the theory suggests that, starting from some critical initial volume fraction ϕ_0, the local nanocluster concentration reaches high enough values, and a condensation phase transition takes place in the proximity of the magnetic poles of the microsphere. Therefore, the opaque regions of the nanoparticle clouds at $\phi_0 \geqslant 0.04\%$ could be interpreted as a liquid-state phase with a high (but not necessarily closely packed) nanocluster concentration.

The effect of the intensity of the external magnetic field on the cloud formation is shown in Fig. 6 for an initial nanoparticle concentration of $\phi_0 = 0.04\%$. As is seen in this figure, the nanoparticle clouds become larger, thicker, and more extended along the magnetic field lines, as the magnetic field intensity increases. This is simply interpreted by increasing the magnetic interactions between the nanoclusters and the microsphere as well as between the nanoclusters themselves. The latter effect could favor the condensation phase transition around the microspheres. Again, the opaque zones of the clouds near the microsphere at $H_0 \geqslant 12$ kA/m likely stand for the liquid-state phase of the nanocluster ensemble. The concentration and magnetic field effects on the cloud size and shape are studied in more detail in Sec. IV C, in conjunction with the theory.

It should be pointed out that, in short-time experiments presented in Figs. 5 and 6, we observed a rather smooth transition between a concentrated, presumably, liquid-state phase of the nanocluster ensemble and a dilute gas-state phase outside the cloud. The absence of a sharp boundary between both phases may come from a polydispersity of the nanocluster suspension: Larger nanoclusters are accumulated in the vicinity of the microsphere, forming a dense liquid-state phase, while smaller nanoclusters form sparse clouds around the latter. In addition to it, nanocluster accumulation is likely a long process hindered by Brownian motion. To check if the equilibrium was reached, we have conducted long-time experiments (3 h), taking special care to avoid degradation of the sample. First, we remark that the distinct boundary between the liquid and the gas phases has only been observed for the most concentrated sample with $\phi_0 = 0.16\%$. Second, the nanocluster accumulation process seems to be achieved for the most dilute sample [$\phi_0 = 0.005\%$, Fig. 7(a)], resulting in relatively small and transparent clouds. For more concentrated suspensions [$\phi_0 = 0.08\%$ and $\phi_0 = 0.16\%$, Figs. 7(b) and 7(c)], the nanoparticle clouds did not cease to grow, at least for 3 h. We also observed the formation of field-induced rodlike aggregates in the bulk of the concentrated suspensions, while these aggregates were not detected in a dilute suspension. Such a phase separation in the two last samples is a long-time process (several hours), and its time scale is similar to the one for the nanocluster accumulation. After a certain elapsed time, sufficient for the formation of long enough aggregates,

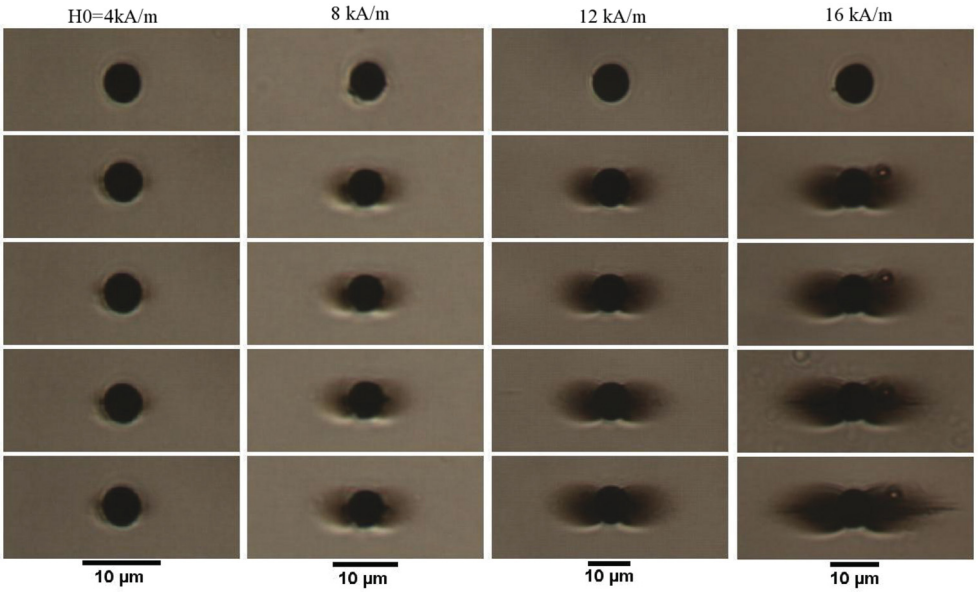

FIG. 6. (Color online) Influence of the magnetic field intensity H_0 on the formation of the nanoparticle clouds in the sterically stabilized (S) nanoparticle suspension. The initial nanoparticle volume fraction is $\phi_0 = 0.04\%$; the image sequence from the top to the bottom corresponds to different elapsed times: 0, 5, 10, 15, and 20 min.

we observed the motion of these aggregates towards the microsphere such that the nanoparticle clouds continued to grow, absorbing the neighboring aggregates. Thus, the cloud growth process could have been stopped only if all the ferrofluid aggregates were absorbed by the clouds, leading to very large clouds whose size depends on the total quantity of nanoclusters in the initial ferrofluid. Such a tendency could be discerned in Fig. 7(c) for a suspension with $\phi_0 = 0.16\%$. In the limit of infinite volume of the nanocluster suspension, the clouds are expected to grow infinitely around the microspheres without reaching thermodynamic equilibrium with ambient suspension. These observations allow us to suppose that infinite cloud growth is associated with the field-induced structuring of the initial nanocluster suspension, while, in the absence of structuring at lower concentrations or magnetic fields, clouds of finite size are expected. Our theory, which is developed in the next section, fully confirms this hypothesis.

In order to understand the influence of the nanoparticle and nanocluster size on their accumulation around microspheres, in Fig. 8 we compared the pictures taken for both (I) and (S) types of synthesized nanoparticles at the same external magnetic field, $H_0 = 16$ kA/m, and at the same initial volume fraction, $\phi_0 = 0.16\%$. The small quasi-isolated nanoparticles of the (I) sample with a mean diameter of about $d \approx 10$ nm build very small halos in the vicinity of the magnetic poles of the microsphere, extended to a distance of about $0.1D$ from the microsphere surface, with $D \approx 5$ μm being the microsphere diameter. On the contrary, the larger nanoclusters of the (S) sample with a mean diameter of about $d \approx 60$ nm build large clouds extended along the magnetic field lines to a distance equal to several microsphere diameters. Such

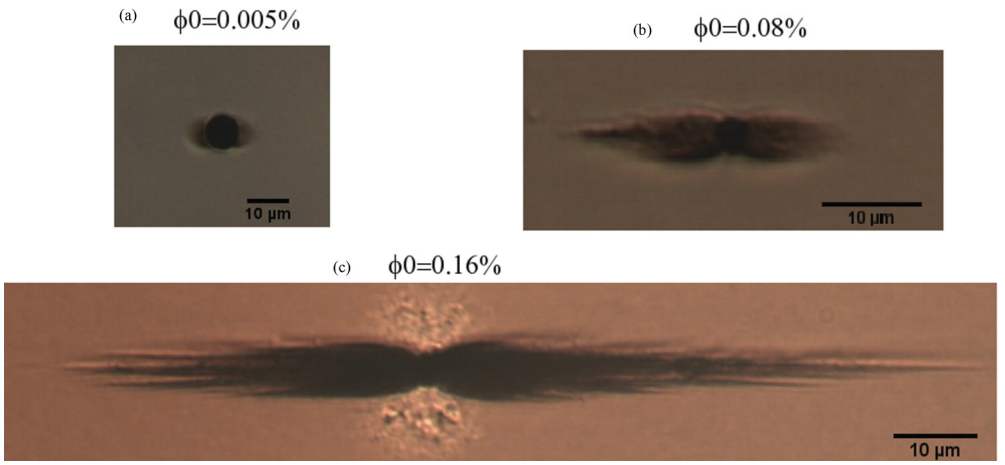

FIG. 7. (Color online) Long-time (3 h) observation of the nanoparticle clouds of the samples (S) at the external magnetic field intensity $H_0 = 8$ kA/m and initial volume fractions $\phi_0 = 0.005\%$ (a), 0.08% (b), and 0.16% (c).

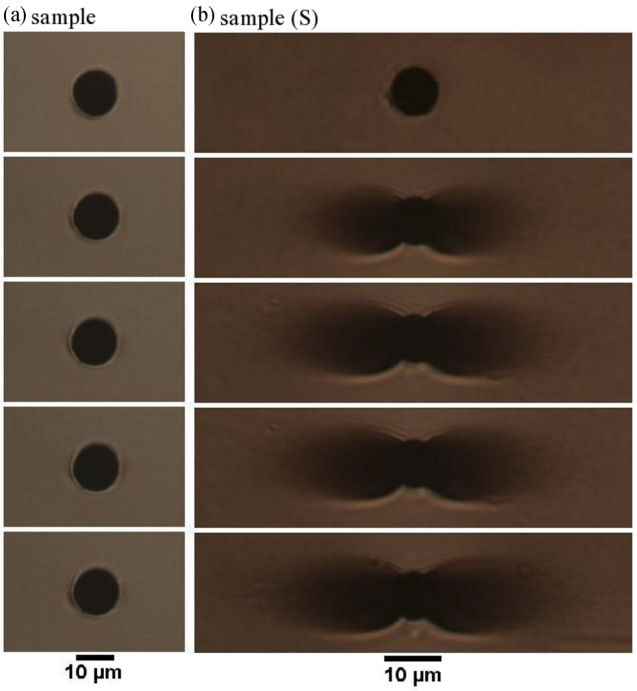

FIG. 8. (Color online) Influence of the nanoparticle (nanocluster) size on the cloud formation at the magnetic field $H_0 = 16$ kA/m and at the initial volume fraction $\phi_0 = 0.16\%$. The left column corresponds to the small size (I)-type nanoparticles ($d^{\mathrm{DLS}} = 11$ mm), and the right column stands for the bigger (S)-type nanoclusters ($d^{\mathrm{DLS}} = 62$ mm). The image sequence from the top to the bottom corresponds to different elapsed times: 0, 5, 10, 15, and 20 min.

a difference comes from the fact that the energy of both nanoparticle-microsphere and nanoparticle-nanoparticle magnetic interactions is proportional to the nanoparticle volume, thus to d^3; these interactions are much more pronounced for bigger (S)-type nanoclusters, leading to a condensation phase transition of nanoclusters in the vicinity of the microspheres.

As a short demonstration of the stabilization of a bimodal non-Brownian magnetic suspension [by the dispersion of micrometer-sized magnetic particles in a dilute (0.16%) aqueous solution of (S)-type nanoclusters], in Fig. 9 we show two nickel microspheres subjected to an external magnetic field, $H_0 = 16$ kA/m, which remained separated from each other at a distance of about ten microsphere diameters thanks to the effective repulsion between overlapping nanoparticle clouds. As already mentioned, such an effect was first discovered by Lopez-Lopez *et al.* [9] and was observed in a relatively concentrated ferrofluid at a nanoparticle volume fraction of about a few percent. In the present work, we reproduced this

FIG. 9. Effective repulsion between two nickel microspheres subjected to an external magnetic field of an intensity $H_0 = 16$ kA/m and parallel to the line connecting the centers of both microspheres. The volume fraction of the (S) nanoclusters is 0.16%.

effect with a dilute ferrofluid composed of large nanoclusters, the ferrofluid being stable to sedimentation.

IV. THEORY AND DISCUSSION

We now develop a thermodynamic theory allowing the prediction of the concentration profiles as well as the size and the shape of the nanoparticle clouds, taking into account interparticle interactions and the eventual gas-liquid phase transition. The thermodynamic state of the nanocluster suspension at each its point is described by a set of intensive thermodynamic variables, such as temperature, particle volume fraction, osmotic pressure, magnetic field intensity, and chemical potential. If the local thermodynamic equilibrium holds, the relationships between these variables (equations of state) do not depend on their space distribution around a microsphere. Therefore, they can be determined by considering an infinite volume of the nanoparticle suspension subjected to an external uniform magnetic field. Using this approach, in Sec. IV A we find the chemical potential and the osmotic pressure of the suspension as functions of the nanocluster volume fraction and the magnetic field intensity. Then, in Sec. IV B, we use these relations to study a gas-liquid phase transition. After that, in Sec. IV C, on the basis of the obtained equations of state and phase diagrams, we calculate the equilibrium concentration profiles of nanoclusters around the microsphere and compare the theory to experimental results. Finally, in Sec. IV D, we develop a pressure balance model and estimate the size and the shape of the clouds in the case of a finite volume of the nanocluster suspension.

A. Thermodynamic variables

Let us consider an infinite volume of homogeneous suspension of sterically stabilized spherical magnetic nanoclusters at a volume fraction $\Phi = \phi/\phi_{\mathrm{int}}$, subjected to an external uniform magnetic field of intensity H_0 (as previously, ϕ and $\phi_{\mathrm{int}} \sim 0.5$ stand for the volume fraction of the nanoparticles in the suspension and the volume fraction of the nanoparticles inside nanoclusters, respectively). We look for the chemical potential of the nanoclusters, $\xi(\Phi, H_0)$, and for the osmotic pressure of the suspension, $p(\Phi, H_0)$. These variables will be found under the following considerations.

(1) The nanoclusters interact with each other via electrostatic and steric repulsion, van der Waals attraction, and magnetic dipolar interactions. Estimations of the intercluster potentials show that the first three interactions are short ranged and the magnetic interaction is long ranged. This allows us to apply a simple approach, in which the nonmagnetic and magnetic interaction potentials give additive and completely independent contributions to the total free energy of the colloid. The contribution of all nonmagnetic terms is therefore approximated by the hard-sphere repulsion that is described by the radial distribution function not altered by the magnetic field, while the magnetic contribution follows from the continuum electrodynamics. Such an approach was successfully used to predict phase transitions in ferrofluids [34] and magnetorheological fluids [35].

(2) We neglect the change in free energy associated with the formation of chains of nanoclusters. This assumption should not seriously contradict the formation of rodlike aggregates

observed experimentally. These aggregates are relatively thick and can, in the simplest case, be regarded as elongated, highly concentrated liquid drops composed of closely spaced but individual nanoclusters [36]. Although the appearance of these aggregates can affect the phase diagram, we shall see in the following that this approximation gives a good enough representation of nanoparticle capture.

(3) For the sake of simplicity, we neglect the size distribution of the nanoclusters and consider all of them to be of the same diameter d, which is taken to be equal to the mean volume diameter, $d^{\mathrm{DLS}} \approx 62$ nm, measured by DLS. Strictly speaking, this assumption is not verified in experiments, so it may induce some errors on the calculated concentration profiles and cloud shapes. The possible effects of the nanocluster polydispersity are briefly discussed below, in conjunction with a comparison of the theory versus the experiments.

Under these approximations, the free energy of a homogeneous suspension composed of N magnetic nanoclusters dispersed in a volume V at a temperature T and subjected to a uniform magnetic field $\mathbf{H}$ is given by the following constitutive relation:

$$F = \left[NkT\ln\left(\frac{N\Lambda^3}{V}\right) - NkT\right] + NkT\Phi\frac{4-3\Phi}{(1-\Phi)^2} - \mu_0\int_0^{\mathbf{H}}\mathbf{m}\cdot d\mathbf{H}, \quad (1)$$

where Λ is the thermal de Broglie wavelength of the nanocluster and $\mathbf{m}$ is the magnetic moment of the whole suspension. The first term on the right-hand side of this equation represents the free energy of an ideal gas of spherical nanoclusters [37], the second term stands for the hard-sphere repulsion between nanoclusters and follows from the Carnahan-Starling theory [25,38], while the last term is the magnetic contribution to the free energy [39], which includes both nanocluster-external field and nanocluster-nanocluster magnetic interactions. The calculation of this term requires further approximations.

(4) As has been stated in Sec. II B, the magnetic nanoclusters, composed of a large number of superparamagnetic nanoparticles, are expected to be paramagnetic, i.e., not having any permanent magnetic moment but being reversibly magnetized by an external magnetic field. Estimations show that the magnetic susceptibility χ_c of the nanoclusters changes by about only 20% within the range of magnetic fields used in our experiments. Therefore, in the first approximation, we consider χ_c to be independent of the applied field and equal to the initial magnetic susceptibility estimated from magnetization measurements, $\chi_c \approx 9$.

(5) Since the magnetic susceptibilities of the nanoclusters and of the suspension (χ_c and χ, respectively) are considered to be isotropic and field independent, the magnetic moment, $\mathbf{m} = \chi\mathbf{H}V$, of the nanocluster suspension is collinear with the magnetic field vector $\mathbf{H}$ and proportional to the magnetic field intensity such that the last term in Eq. (1) takes the following form: $-\mu_0\int_0^{\mathbf{H}}\mathbf{m}\cdot d\mathbf{H} = -(1/2)\mu_0\chi H^2 V$, with $H = |\mathbf{H}|$.

(6) The full definition of the free energy requires a specific expression for the magnetic susceptibility χ of the colloid as a function of its concentration, which should correctly account for magnetic interactions between nanoclusters. A great number of effective medium theories have been proposed for calculations of the effective dielectric and magnetic properties of composite materials (see, for instance, Refs. [40] and [41]). The most popular Maxwell-Garnett theory was found to strongly underestimate the magnetic susceptibility of composites at high concentrations. Therefore, we choose the theory of Looyenga-Landau-Lifshitz [39,42], which was initially derived for composites with a low dielectric and magnetic contrast but found to be reasonably accurate for the dielectric and magnetic inclusions with a moderate susceptibility (generally less than ten) in a wide concentration range (see Ref. [43] and Table 6 in Ref. [41]). This theory gives the following expression for the magnetic susceptibility χ of the nanocluster suspension:

$$(\chi+1)^{1/3} = \Phi(\chi_c+1)^{1/3} + (1-\Phi)(\chi_s+1)^{1/3}, \quad (2)$$

where $\chi_s \approx 0$ is the magnetic susceptibility of the solvent (water).

Finally, using the standard thermodynamic relations, we derive the following equations for the chemical potential ξ and the osmotic pressure p of the suspension:

$$\xi = \left(\frac{\partial F}{\partial N}\right)_{T,V,H} = V_c\left(\frac{\partial(F/V)}{\partial\Phi}\right)_{T,H} = kT\left[\ln\frac{\Lambda^3}{V_c} + \ln\Phi + \Phi\frac{8-9\Phi+3\Phi^2}{(1-\Phi)^3} - \alpha\frac{\partial\chi}{\partial\Phi}\right], \quad (3)$$

$$p = -\left(\frac{\partial F}{\partial V}\right)_{T,N,H} = -\frac{F}{V} + \Phi\left(\frac{\partial(F/V)}{\partial\Phi}\right)_{T,H} = \frac{kT}{V_c}\left[\Phi\frac{1+\Phi+\Phi^2-\Phi^3}{(1-\Phi)^3} - \alpha\Phi^2\frac{\partial(\chi/\Phi)}{\partial\Phi}\right], \quad (4)$$

with $V_c = \pi d^3/6$ being the nanocluster volume and $\alpha = (\mu_0 H^2 V_c)/(2kT)$ the magnetic field parameter characterizing the ratio of the nanocluster magnetic energy to the thermal energy. While deriving the last two equations, we took into account that the number density of nanoclusters is related to their volume fraction via the expression $N/V = \Phi/V_c$. The last terms in brackets on the right-hand sides of Eqs. (3) and (4) stand for the magnetic contributions to the chemical potential and the osmotic pressure, respectively, and are easily obtained by replacing the magnetic susceptibility χ by the one found from Eq. (2), which yields $\partial\chi/\partial\Phi = 3y(1+\Phi y)^2$ and $\Phi^2\partial[\chi/\Phi]/\partial\Phi = y^2\Phi^2(3+2\Phi y)$ with $y = (\chi_c+1)^{1/3} - 1$.

B. Phase transition

Beyond some critical magnetic field, the concentration dependencies of the chemical potential [Eq. (3)] and of the osmotic pressure [Eq. (4)] appear to be nonmonotonically increasing. They have an N shape with a decreasing branch at intermediate concentrations, similar to that of the van der Waals gas and inherent for a gas-liquid phase transition. The equilibrium phase behavior in the nanocluster suspension will be governed by the equality of temperatures, chemical

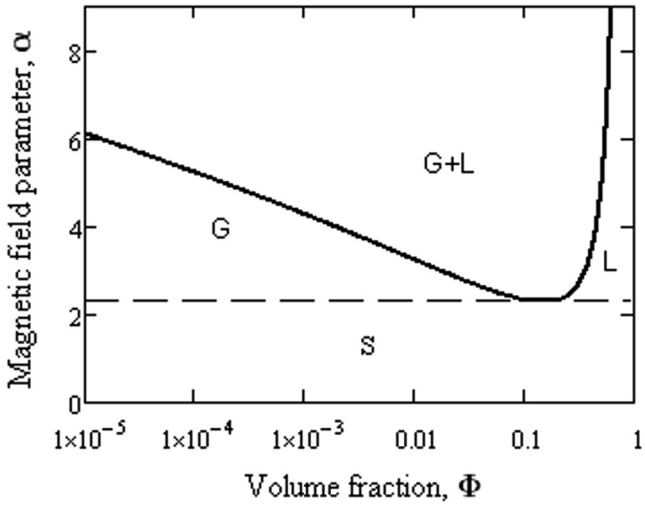

FIG. 10. α-Φ phase diagram of the suspension of magnetite nanoclusters. The two curves divide the phase diagram into four regions (L, liquid state; G, gas state; L + G, gas-liquid mixture; and S, supercritical state), at which no condensation phase transition occur whatever is the particle volume fraction. The dashed curve corresponds to the critical magnetic field $\alpha_c \approx 2.3$; this curve is similar to the critical isotherm of a van der Waals gas.

potentials, and osmotic pressures in both phases [29,37]. Thus, in our isothermal nanocluster suspension, the binodals (curves corresponding to the coexistence of both phases) of the gas-liquid equilibrium will be defined by the following transcendental equations:

$$\xi(\Phi_L,\alpha) = \xi(\Phi_G,\alpha), \tag{5a}$$

$$p(\Phi_L,\alpha) = p(\Phi_G,\alpha), \tag{5b}$$

where the subscripts L and G stand for the liquid and gas phases, respectively.

The system of two equations (5) is solved numerically with respect to the two unknowns, Φ_L and Φ_G, and both binodal concentrations are found as functions of the magnetic field parameter α. The α-Φ phase diagram is plotted in Fig. 10 for nanoclusters with a magnetic susceptibility of $\chi_c = 9$. The critical point is identified as the minimum of the binodal curve and corresponds to the magnetic field parameter $\alpha_c \approx 2.3$ and to the nanocluster volume fraction $\Phi_c \approx 0.13$. Similar to the case of the van der Waals gas, both the binodal curve and the curve $\alpha = \alpha_c$ divide the phase diagrams into four regions corresponding to a gas phase, a liquid phase, a gas-liquid mixture, and a supercritical state existing at low magnetic fields, $0 \leqslant \alpha \leqslant \alpha_c$, at which the condensation phase transition does not occur. As is seen in Fig. 10, the left branch of the binodal curve has a relatively small slope such that the gas-liquid phase transition may occur at relatively low volume fractions of nanoclusters, $\Phi < 10^{-4} = 0.01\%$, at the parameter $\alpha > 4$ corresponding to magnetic fields as small as $H > 14.5$ kA/m.

C. Nanoparticle clouds: The thermodynamic model

Consider now a magnetizable microsphere of radius a, introduced into an infinite volume suspension of sterically stabilized nanoclusters and subjected to an external uniform magnetic field $\mathbf{H}_0$, as depicted in Fig. 11. The polar coordinate system (r,θ) is introduced in such a way that its origin coincides with the microsphere center and the angle θ is counted in the counterclockwise direction from the magnetic field vector $\mathbf{H}_0$.

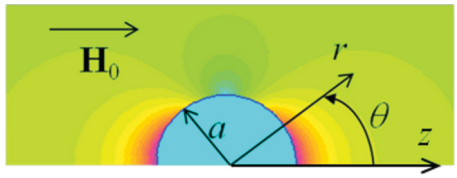

FIG. 11. (Color online) Sketch of the problem geometry. Distribution of the magnetic field intensity [according to (6)] around a microsphere is shown schematically by different colors.

We look for the concentration profile $\Phi(r,\theta)$ of the nanoclusters around the microsphere as well as for the shape of the nanocluster cloud, using the following assumptions and considerations.

(1) The microsphere is supposed to be made of a magnetically soft material of high magnetic susceptibility, $\chi_{ms} \sim 100$ (as nickel in our experiments). The magnetic susceptibility χ of the medium surrounding the microsphere varies from point to point as a function of the nanocluster concentration Φ. It takes the maximum value in the vicinity of the magnetic poles of the microsphere and minimum near the microsphere equator. Using Eq. (2), these values are estimated to be $\chi_{max} \approx 4$ and $\chi_{min} \approx 0$. Thus, the magnetic contrast between the microsphere and the surrounding medium remains very high at any point of the latter, which allows us to neglect, at the first approximation, the spatial variation of the magnetic susceptibility χ and to apply the well-known relations for the magnetic field distribution around a magnetized sphere [26]:

$$H_r = H_0\left(1 + \frac{2\beta}{r^3}\right)\cos\theta, \quad H_\theta = -H_0\left(1 - \frac{\beta}{r^3}\right)\sin\theta, \quad H = \sqrt{H_r^2 + H_\theta^2}, \tag{6}$$

where $\beta = (\chi_{ms} - \chi)/(\chi_{ms} + 2\chi + 3) \approx 1$ is the magnetic contrast factor approximately equal to unity. Using the last equations, we can assign the magnetic field parameter $\alpha(r,\theta) = [\mu_0 H(r,\theta)^2 V_c]/(2kT)$ to any point (r,θ) around a microsphere.

(2) At local thermodynamic equilibrium, the chemical potential ξ and the osmotic pressure p are defined at any point of the nanocluster suspension as functions of the local concentration $\Phi(r,\theta)$. These functions are given by Eqs. (3) and (4) for any thermodynamic state of the suspension except for the gas-liquid mixture. The latter is characterized by the so-called condensation plateau, for which both the osmotic pressure and the chemical potential are independent of the nanocluster concentration at a given fixed magnetic field intensity H. For a better understanding, we plot two curves of the constant magnetic field ($\alpha = 3$ and $\alpha = 3.90$) in the ξ-Φ phase diagram in Fig. 12(a). These curves show an initial increase of the chemical potential with concentration in the gas phase, a condensation plateau in the gas-liquid mixture region, and a final steep increase in the liquid phase, whose

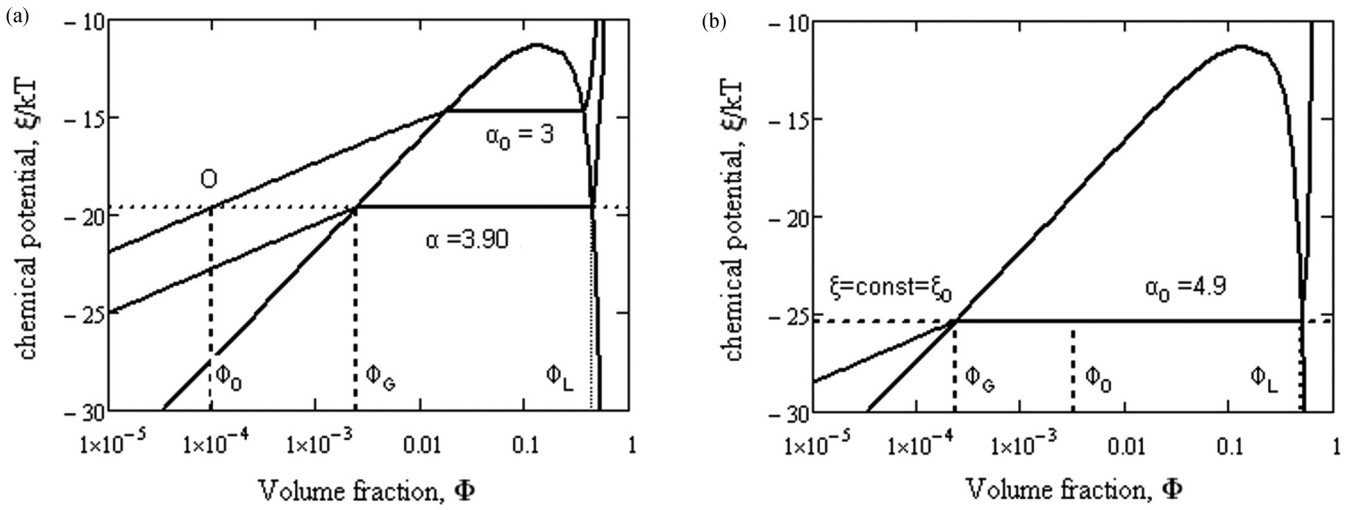

FIG. 12. Determination of the critical field along the cloud boundary with the help of the phase diagrams ξ-Φ. (a) corresponds to the situation where the initial nanocluster concentration Φ_0 is too low to induce the phase transition in the nanocluster suspension at infinity from the microsphere. Nevertheless, the magnetic field near the microsphere is high enough to induce condensation of the nanoclusters and the formation of a dense liquid-state phase around the microsphere. (b) corresponds to the initial nanocluster concentration Φ_0 that is high enough to induce the phase separation at infinity from the microsphere. Infinite clouds are expected in infinite volume nanocluster suspension. In reality, finite volume clouds will appear in a large but finite volume suspension, and their shape is defined by the pressure balance model (Sec. IV D).

shapes are qualitatively similar to the ones of the van der Waals isotherms.

(3) The nanocluster suspension reaches local thermodynamic equilibrium when its chemical potential becomes homogeneous over the whole volume, $\xi(r,\theta) = \text{const}$ [37]. In the infinite volume suspension, the concentration of nanoclusters at infinity from the microsphere remains unchanged and is equal to the initial concentration Φ_0 in the absence of the magnetic field. This explicitly determines the chemical potential at infinity, $\xi_0 \equiv \xi(\Phi_0,\alpha_0)$, and allows one to calculate the nanocluster concentration $\Phi(r,\theta)$ at any point by the following relation:

$$\xi(\Phi(r,\theta),\alpha(r,\theta)) = \text{const} = \xi(\Phi_0,\alpha_0), \tag{7}$$

with $\alpha_0 = (\mu_0 H_0^2 V_c)/(2kT)$ being the magnetic field parameter at infinity, corresponding to the external magnetic field H_0. The concentration $\Phi(r,\theta)$ is obtained by a numerical solution of Eq. (7) together with Eqs. (6) and (3) for both gas and liquid phases of the nanocluster ensemble.

Dense nanoparticle clouds around a microsphere are associated with the liquid phase of the nanocluster ensemble, while the dilute regions around the clouds correspond to the gas state. To find the shape of the nanoparticle cloud or rather the interface between the liquid and the gas phases, we should state the difference between the two following cases: (1) The condensation phase transition does not occur at infinity from the microsphere but does at some finite distance from the microsphere; and (2) the condensation phase transition occurs at infinity. As we shall see, in the former case, finite-sized nanoparticle clouds are formed, while in the latter case, the local thermodynamic equilibrium cannot be achieved since phase separation can occur everywhere in the suspension and the drift of the condensed domains towards the microparticle is too slow to reach equilibrium. The second case is considered in more detail in Sec. IV D. Now, we shall focus on the first case, for which the magnetic field intensity H_0 and the nanocluster initial concentration Φ_0 are not high enough to induce condensation at infinity from the microsphere, so the nanocluster ensemble is in the gas state there.

When approaching the magnetic poles of the microsphere, the magnetic field intensity H increases progressively until some critical value H_c at which the gas-liquid transition occurs. Of course, both the magnetic field and the osmotic pressure are not continuous on the interface between the gas and liquid phases (cloud surface) because of the difference in magnetic susceptibilities of these phases. So, the condition of the mechanical equilibrium of both phases [Eq. (5b)] should contain a magnetic pressure jump, which depends on the magnetic field orientation relative to the interface. Thus, the osmotic pressure should vary from point to point along the interface. The problem becomes computationally complicated and requires a simultaneous solution of the Maxwell equations for the magnetic field distribution and the phase equilibrium equations for the unknown gas-liquid interface. Therefore, in the frame of this model, we neglect the magnetic field jump and the pressure jump on the cloud interface that nevertheless will allow us to obtain a reasonable semiquantitative agreement with experimental results (some improvement on the model taking into account the magnetic pressure jump will be presented in Sec. IV D). The interface between the gas and liquid phases (the surface enclosing the nanoparticle cloud) is defined as the surface of the constant absolute value of the critical magnetic field H_c corresponding to the phase transition. The latter can be found from the condition of the equality of the chemical potential at infinity and on the cloud surface:

$$\xi(\Phi_L(\alpha_c),\alpha_c) = \xi(\Phi_0,\alpha_0), \tag{8a}$$

$$\xi(\Phi_G(\alpha_c),\alpha_c) = \xi(\Phi_0,\alpha_0), \tag{8b}$$

where α_c is the magnetic field parameter corresponding to the critical magnetic field H_c, and $\Phi_L(\alpha_c)$ and $\Phi_G(\alpha_c)$ are the nanocluster concentrations at the internal and external sides of the cloud interface, respectively (in the liquid phase and in the gas phase). Since the chemical potential is the same in both phases, the two last equations are completely equivalent and one of them must be solved with respect to α_c. As a result, the critical magnetic field α_c is found as a function of the initial concentration Φ_0 and the external magnetic field α_0.

The critical field can also be determined graphically from the ξ-Φ phase diagram plotted in Fig. 12(a). First, from Φ_0 and α_0, we calculate ξ_0, the chemical potential far from the microsphere. The values Φ_L and Φ_G are then found by the intersection of the $\xi = \xi_0$ curve [the dashed horizontal line in Fig. 12(a)] with the binodal curves, and α_c is the value of $\alpha = \text{const}$ curve, whose condensation plateau coincides with the $\xi = \xi_0$ line. The difference $\Phi_L - \Phi_G$ represents the concentration jump on the cloud surface. This surface is symmetric with respect to the microsphere axis parallel to the external magnetic field vector $\mathbf{H}_0$ and is described by a geometric locus $[R(\theta),\theta]$ in the polar coordinates. The function $R(\theta)$ can be found from the critical magnetic field with the help of the expression $\alpha(R(\theta),\theta) = \alpha_c(\Phi_0,\alpha_0)$. Substituting Eq. (6) with $\beta = 1$ for the magnetic field distribution into the last expression, we find the equation of the cloud surface in its final form:

$$R(\theta) = \left[\frac{1 + 3\cos^2\theta}{(1 - 3\cos^2\theta) + [(1 - 3\cos^2\theta)^2 + (1 + 3\cos^2\theta)(\alpha_c/\alpha_0 - 1)]^{1/2}}\right]^{1/3}. \quad (9)$$

The shape, $R(\theta)$, of the nanoparticle cloud around a microsphere, found numerically from Eq. (9), is presented in Fig. 13 for the initial nanocluster concentration $\Phi_0 = 0.08\%$ (corresponding to the nanoparticle volume fraction $\phi_0 = \Phi_0\phi_{\text{int}} \approx 0.04\%$), and the external magnetic fields $H_0 = 4$ and 12 kA/m. At the lowest magnetic field, $H_0 = 4$ kA/m, the nanoparticle cloud appears to be very small, extending to a distance about $0.2a$ from the microsphere surface. At a higher magnetic field, $H_0 = 12$ kA/m, the cloud is much larger and extends to a distance of $1.7a$ from the collector. For the given parameters, the calculated cloud shape qualitatively reproduces the shape observed in experiments (cf. the first and third columns of Fig. 6).

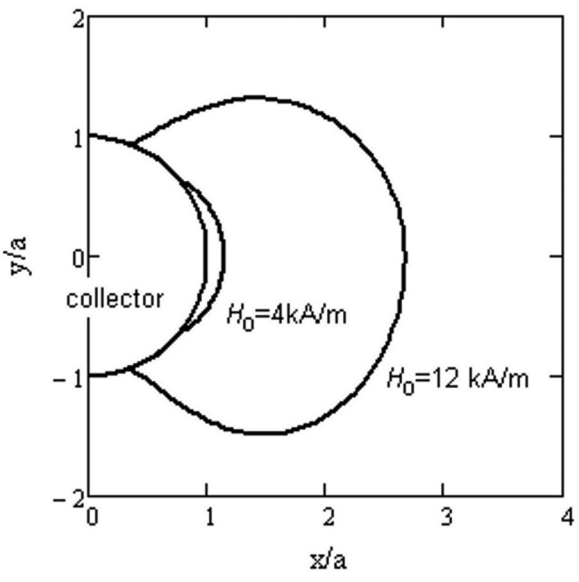

FIG. 13. Shape of nanoparticle clouds calculated by the thermodynamic model [Eq. (9)]. The initial volume fraction of nanoclusters is $\Phi_0 = 0.08\%$, corresponding to the nanoparticle volume fraction $\phi_0 = 0.04\%$.

The nanocluster concentration profiles along and across the direction of the applied magnetic field are presented in Figs. 14(a) and 14(b), respectively, at the same set of parameters, $H_0 = 4$ and 12 kA/m, $\Phi_0 = 0.08\%$. We see that, at $H_0 = 12$ kA/m, when moving away from the microsphere along the magnetic field direction, the concentration decreases quasilinearly inside the cloud (liquid phase), then it drops significantly on the cloud interface down to $\Phi = 0.7\%$, and decreases gradually outside the cloud (gas phase), tending asymptotically to the initial value $\Phi_0 = 0.08\%$ at infinity [Fig. 14(a)]. At the magnetic field $H_0 = 4$ kA/m, the concentration profile is smoother and the concentration jump on the cloud interface appears to be much smaller than for $H_0 = 12$kA/m. This is explained by the fact that the condensation plateau at smaller magnetic fields is closer to the critical point and therefore is shorter, giving a smaller concentration jump $\Phi_L - \Phi_G$ [cf. Fig. 12(a)]. Figure 14(b) reveals that the nanocluster concentration near the microsphere equator is lower than the initial concentration Φ_0 at infinity. This is easily explained by a repulsive magnetic interaction in this region. When moving apart from the microsphere surface in the direction perpendicular to the applied magnetic field, the magnetic field intensity increases progressively from zero on the microsphere equator to H_0 at infinity [cf. Eq. (6)] such that the nanocluster concentration also increases with the distance r in this direction [Fig. 14(b)]. The concentration exhibits a more rapid increase at lower magnetic field, $H_0 = 4$ kA/m, because the repulsive magnetic interaction between nanoclusters and the microsphere is smaller for this field, compared to the one for $H_0 = 12$ kA/m.

The contour plot of the calculated two-dimensional (2D) concentration profiles is shown in Fig. 15 for the nanocluster concentration $\Phi_0 = 0.08\%$ and for the external magnetic field $H_0 = 12$ kA/m. To compare with experiments, we add the corresponding optical microscopy picture at the bottom of the figure. The intensity of the transmitted light of the experimental picture could serve as a qualitative measure of the nanoparticle concentration. As already mentioned, it was

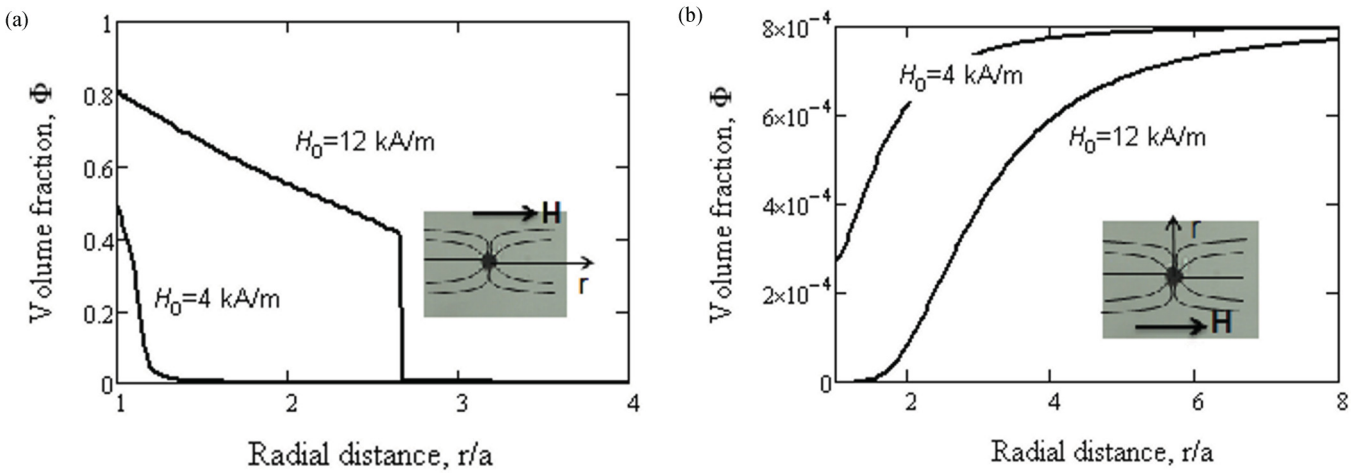

FIG. 14. (Color online) Concentration profile of the nanocluster suspension near the magnetic collector: (a) along the direction of the applied magnetic field; (b) perpendicularly to the direction of the applied field. The initial volume fraction of the nanoclusters is $\Phi = 0.08\%$, corresponding to the nanoparticle volume fraction $\phi_0 = 0.04\%$.

impossible to establish reliable relationships between the light intensity and the concentration because of the opacity of the high concentration regions where the Beer-Lambert law does not apply. We can compare theoretical and experimental concentration profiles only qualitatively. According to our theory, at a high enough magnetic field intensity, the concentration inside the cloud appears to be one to two orders of magnitude higher than the concentration outside the cloud, so a sharp and well-defined cloud border is predicted. However, in the experiments, the particle concentration seems to vary smoothly without substantial jumps, even though opaque regions near the microsphere surface are well distinguishable. Such an inconsistency could probably come from the polydispersity of the nanocluster suspension: As already stated, larger

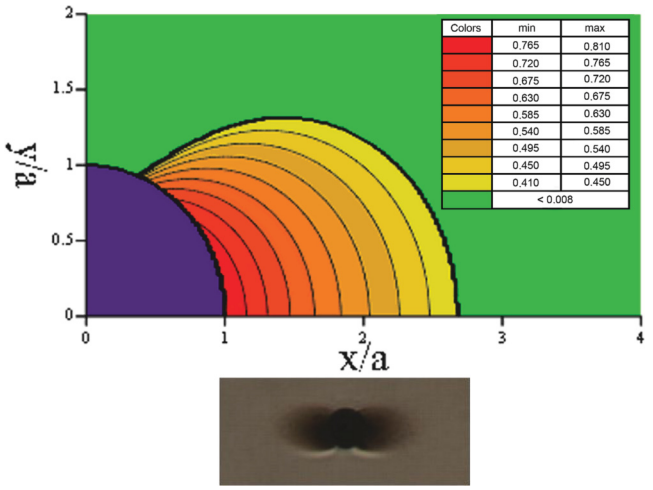

FIG. 15. (Color online) Calculated nanocluster concentration profile around a microsphere for the initial nanocluster concentration $\Phi_0 = 0.08\%$ (nanoparticle concentration $\phi_0 = 0.04\%$) and the external magnetic field $H_0 = 12$ kA/m. The color legend corresponds to the local nanocluster concentrations $\Phi(r,\theta)$ shown in absolute values (not in percent). The nanoparticle cloud observed experimentally at the same parameters, Φ_0 and H_0, is shown on the bottom of the figure.

nanoclusters are accumulated in the vicinity of the microsphere, forming a dense, liquidlike phase, while smaller nanoclusters form sparse clouds around the latter. So, taking into account the nanocluster polydispersity in the model could improve the agreement between theory and experiments.

To quantify the cloud size and provide a quantitative comparison between the experiments and the theory, we define the longitudinal cloud size as the length of a line segment between the microsphere surface and the point along the z axis (Fig. 11) where the transmitted light intensity was 10% smaller than the mean intensity far from the cloud. The concentration dependence of the cloud longitudinal size is reported in Fig. 16(a) for the magnetic field $H_0 = 14$–16 kA/m, and the magnetic field dependence of the cloud size is shown in Fig. 16(b) for the initial nanoparticle volume fraction $\phi_0 = 0.04\%$ corresponding to the nanocluster concentration $\Phi_0 = \phi_0/\phi_{\rm int} \approx 0.08\%$. Both experiment and theory show an increase in cloud size with the initial particle concentration and the magnetic field intensity. This is easily explained by concentration and field enhancement of the dipolar interactions between nanoclusters, leading to their condensation around a microsphere. As is seen in Figs. 16(a) and 16(b), the theory reveals a divergence of the cloud size at high enough magnetic fields and nanoparticle concentrations. This corresponds to an infinite growth of clouds starting from some threshold values of H_0 and ϕ_0. Such a divergence is also confirmed in experiments. For example, the experimental cloud size exhibits a drastic jump from $L/a \approx 5$ at $\phi_0 \approx 0.08\%$ to $L/a \approx 25$ at $\phi_0 \approx 0.16\%$ [the last point is not shown in Fig. 16(a)]. Beyond the threshold values of H_0 and ϕ_0, the cloud sizes and shapes cannot be found by the present model anymore, and another approach will be developed below for their determination.

D. Nanoparticle clouds: The pressure balance model

At high enough external magnetic fields and nanocluster volume fractions, the condensation phase transition in the nanocluster suspension may occur at an infinite distance from the

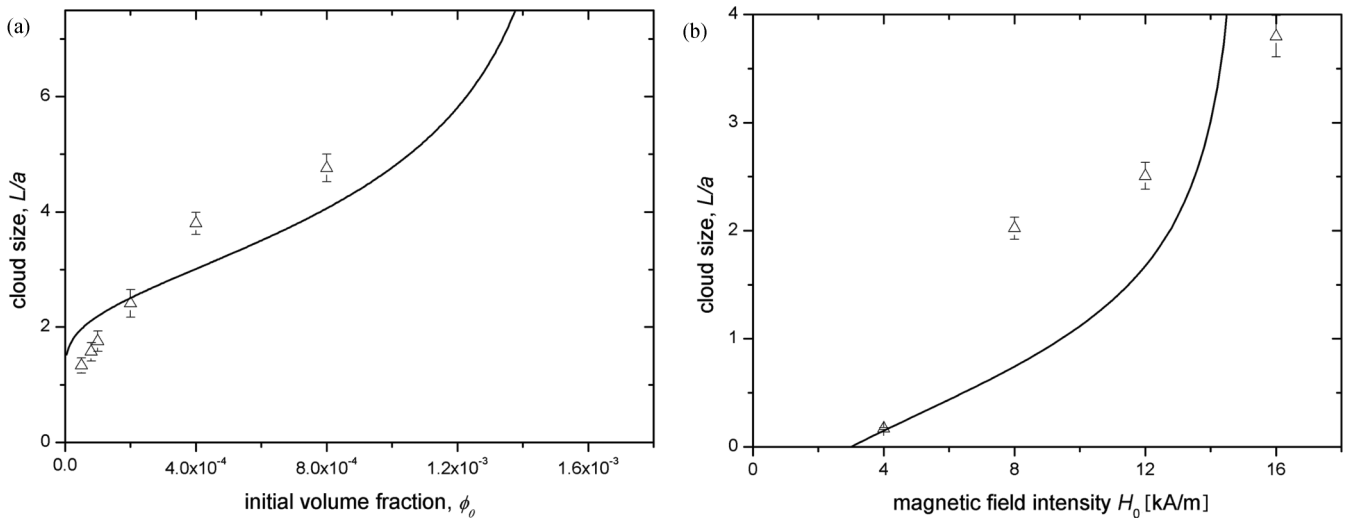

FIG. 16. Theoretical (solid curve) and experimental (points) dependencies of the cloud longitudinal size on the initial particle volume fraction at $H_0 = 16$ kA/m (a) and on the magnetic field intensity at $\phi_0 = 0.04\%$ (b). The experimental points correspond to an elapsed time of 20 min.

magnetic microsphere. As already mentioned, this phase transition is manifested by the appearance of rodlike aggregates composed of ferrofluid nanoclusters, with these aggregates often being considered as elongated concentrated ferrofluid droplets. If the applied magnetic field is spatially uniform, the coexistence between the concentrated phase (droplets) and the dilute phase (isolated nanoclusters) is possible in the whole volume of the nanocluster suspension, provided that the droplet size distribution is governed by the free energy minimum [44]. However, in the case of an inhomogeneous magnetic field around a microsphere, all the droplets will precipitate to the regions of the higher magnetic fields and coalesce into a single large concentrated drop around the microsphere. Thus, infinitely large nanoparticle clouds are expected to form in an infinite volume of the nanocluster suspension.

If the nanocluster suspension volume is not infinitely large, the amount of nanoclusters condensed around a magnetic microsphere will depend on the total amount of nanoclusters in the initial suspension, i.e., on its volume and initial volume fraction. We shall now estimate the volume and shape of the nanoparticle clouds around a single microsphere placed in a large but finite volume V of the nanocluster suspension exhibiting a gas-liquid phase transition far from the microsphere. This situation is realized in visualization experiments when a drop of a bimodal mixture of the magnetic microspheres with nanoclusters is sandwiched between two glass plates. If the volume fraction $\phi_{\rm ms}$ of microspheres is known, the nanocluster suspension volume per one microsphere is $V_1 = V_{\rm ms}/\phi_{\rm ms}$, where $V_{\rm ms} = 4\pi a^3/3$ is the microsphere volume.

In this model, we shall take into account the magnetic pressure jump on the cloud surface. As already mentioned, the exact solution of this problem requires simultaneous determination of the magnetic field distribution, of the phase equilibrium conditions on the cloud interface, and of the cloud volume that necessitates substantial numerical efforts. At this stage, we restrict our analysis to estimations made under the following approximations and considerations.

(1) Once the external magnetic field is applied, the nanocluster droplets appear in the whole suspension volume and begin to migrate towards the microsphere. During time, the volume of the liquid phase around a microsphere increases and the concentration of the dilute gas phase outside the cloud decreases, keeping the total amount of nanoclusters constant. The migration of droplets will stop when the nanocluster concentration in the dilute phase becomes small enough to prevent condensation (and, consequently, the formation of droplets) outside the cloud. The concentrations Φ_G and Φ_L in the dilute and the dense phases are estimated as the binodal concentrations at the two extremities of the condensation plateau at the external field H_0 [or α_0; cf. Fig. 12(b)]. The values $\Phi_L(\alpha_0)$ and $\Phi_G(\alpha_0)$ are found by numerical solution of the system of Eqs. (5a) and (5b).

(2) The cloud volume is calculated by an iterative procedure. At the first iteration, we neglect the concentration variations and assume that the nanocluster concentration is equal to $\Phi_L(\alpha_0)$ and $\Phi_G(\alpha_0)$ at any point inside the cloud (dense phase) or outside the cloud (dilute phase), respectively. Since the total volume of the nanoclusters is kept constant, the cloud volume is defined by the following relation:

$$V_L = V_1 \frac{\Phi_0 - \Phi_G}{\Phi_L - \Phi_G}. \tag{10}$$

(3) Now we shall take into account the concentration variation inside the cloud. The shape of the cloud surface is found from the condition of its mechanical equilibrium, assuming continuity of the normal stress across the surface [45]. The stress tensor in the dense phase of the nanocluster suspension is given by the following equation [46]:

$$\sigma_{ik} = -\left\{P + \mu_0 \int_0^H \left[M - \Phi\left(\frac{\partial M}{\partial \Phi}\right)_{T,H}\right] dH\right\}\delta_{ik} - \frac{1}{2}\mu_0 H^2 \delta_{ik} + H_i B_k = -p_{\rm tot}\delta_{ik} - \frac{1}{2}\mu_0 H^2 \delta_{ik} + H_i B_k, \tag{11}$$

where $M = \chi H$ is the magnetization of the nanocluster suspension, δ_{ik} is the delta Kronecker, $P = -(\partial F_0/\partial V)_T$ is the pressure in the nanocluster suspension defined through the nonmagnetic term F_0 of the free energy and including both contributions from the solvent molecules and the nanoclusters, $p_{\rm tot}$ is a so-called total pressure of the suspension equal to the sum of the pressure P, and the magnetic osmotic pressure (the integral term in curly brackets).

From now, we shall neglect a small nanocluster concentration outside the cloud. So, neglecting magnetic properties of the dilute phase as well as the capillary pressure, the pressure jump across the cloud surface follows directly from Eq. (11) [46]:

$$p_{\rm tot\,}{}_G - p_{\rm tot\,}{}_L = \tfrac{1}{2}\mu_0 M_n^2 = \tfrac{1}{2}\mu_0 \chi^2 H_n^2, \tag{12}$$

with $p_{\rm tot}{}_G$ and $p_{\rm tot}{}_L$ being the total pressure in the gas and liquid phases (outside and inside the cloud, respectively), M_n and H_n are the normal components of the magnetization and of the magnetic field on the internal side of the cloud interface, and $\chi = \chi(\Phi)$ is the magnetic susceptibility on the internal side of the cloud surface, whose concentration dependency will be defined below.

Since we neglect the nanocluster concentration Φ_G outside the cloud, the total pressure $p_{\rm tot}{}_G$ in the dilute phase is considered to be constant at any point outside the cloud. The total pressure $p_{\rm tot}{}_L$ in the dense phase varies from point to point according to the following equation [46]:

$$\nabla \cdot \boldsymbol{\sigma} = 0 \Rightarrow \nabla p_{\rm tot\,}{}_L = \mu_0 M \nabla H, \tag{13}$$

which gives, after the integration along the cloud surface,

$$p_{\rm tot\,}{}_L - p^*_{\rm tot\,}{}_L = \mu_0 \int_{H*}^{H(r,\theta)} M dH = \mu_0 \int_{H*}^{H(r,\theta)} \chi H dH, \tag{14}$$

where $p^*_{\rm tot\,}{}_L$ and H^* are the total pressure and the magnetic field intensity in the liquid phase at some reference point on the cloud surface, chosen to be on the microsphere surface, i.e., at $r = 1$ and $\theta = \theta^*$ (the angle θ^* will be found later); $H(r,\theta)$ is the magnetic field intensity at any other point (r,θ) on the internal side of the cloud surface.

We suppose that the cloud surface intersects the microsphere surface at a right angle. On the other hand, on the surface of a strongly magnetized microsphere, the magnetic field lines also make a right angle with its surface. Both of these conditions indicate that the pressure jump across the cloud surface at the reference point $(1,\theta^*)$ is zero, $p^*_{\rm tot\,}{}_G - p^*_{\rm tot\,}{}_L = 0$, as follows from Eq. (12). Thus, combining this last result with Eqs. (12) and (14), we arrive, after some rearrangement, to the following expression:

$$-\int_{H^*}^{H(r,\theta)} \chi H dH = \frac{1}{2}\chi^2 H_n^2. \tag{15}$$

In this last equation, the magnetic susceptibility $\chi = \chi(\Phi)$ on the internal side of the cloud interface depends on the nanocluster volume fraction Φ on the interface, and consequently on the magnetic field intensity on the cloud surface. As explained previously, the concentration is found from the equilibrium of the chemical potential at any point of the cloud surface with the chemical potential at infinity:

$$\xi(\Phi,\alpha) = \text{const} = \xi(\Phi_0,\alpha_0). \tag{16}$$

Note that the chemical potential at infinity is defined in this case by the condensation plateau in the ξ-Φ phase diagram [Fig. 12(b)]. Equation (16) should be solved with respect to Φ, which gives the concentration $\Phi(\alpha,\alpha_0,\Phi_0)$ as a function of a certain magnetic field α on the cloud surface, the magnetic field α_0 at infinity, and the initial concentration Φ_0. The magnetic susceptibility $\chi(\alpha)$ [or, equivalently, $\chi(H)$] is then found as a function of the magnetic field α (or H) upon replacing Φ in Eq. (2) by $\Phi(\alpha,\alpha_0,\Phi_0)$.

Let $R(\theta)$ be the equation describing the geometrical shape of the nanoparticle cloud. We suppose that the magnetic field distribution inside the cloud is still given by Eq. (6). Using this equation for the magnetic field intensities H^* and $H(r,\theta)$ and expressing the normal component of the magnetic field $H_n(r,\theta) = H_r n_r + H_\theta n_\theta$ through the components of the unit vector **n** normal to the cloud surface, we arrive at the following differential equation for the cloud surface:

$$-\frac{2}{\chi^2}\int_{h^*}^{h} \chi(h) h dh = \frac{(h_r - h_\theta R'/r)^2}{1 + (R'/r)^2}, \tag{17}$$

where the following notations are introduced: $R' \equiv dR/d\theta$, $h^* = H^*/H_0 = 3\cos\theta^*$, $h_r = H_r/H_0 = (1 + 2/r^3)\cos\theta$, $h_\theta = H_\theta/H_0 = -(1 - 1/r^3)\sin\theta$, $h = H/H_0 = \sqrt{h_r^2 + h_\theta^2}$. Equation (17) should be solved with respect to the function $R(\theta)$ under the initial condition $R(\theta^*) = 1$ and with $\chi(h)$ defined above with the help of Eq. (16). The last unknown parameter, the angle θ^*, is found from the previously defined cloud volume [cf. Eq. (10)] using the following relation:

$$V_L = 2\frac{2\pi}{3}\int_0^{\theta^*} \sin\theta [R^3(\theta) - 1] d\theta, \tag{18}$$

where the factor 2 before $2\pi/3$ stands for the two clouds attached to the north and the south magnetic poles of the microsphere.

The nanocluster concentration profile inside the cloud is calculated using the condition of homogeneity of the chemical potential, i.e., solving Eq. (7) with respect to Φ at a given position (r,θ) inside the cloud. At the second iteration, we recalculate the volume of the cloud V_L by replacing the concentration Φ_L in Eq. (10) by the mean value $\langle\Phi_L\rangle = (1/V_L)\int \Phi dV$ of the concentration inside the cloud, issued from the first iteration. The iterations on V_L are pursued until convergence.

The concentration profile and the cloud surface calculated numerically from Eqs. (16)–(18) are shown in Fig. 17 for the external magnetic field $H_0 = 16$ kA/m ($\alpha_0 = 4.9$) and the initial nanoparticle volume fraction $\phi_0 = 0.16\%$ ($\Phi_0 \approx 0.32\%$). The nanoparticle cloud observed experimentally at the same parameters, ϕ_0 and H_0, is shown on the bottom of Fig. 17.

Using Eq. (10), we estimate the volume of the clouds around a microsphere to be about 11 times the microsphere volume. Both the calculated and the experimentally observed shapes of the nanoparticle clouds appear to be strongly extended along the magnetic field lines trying to minimize their magnetostatic energy. The quantitative agreement between the theory and

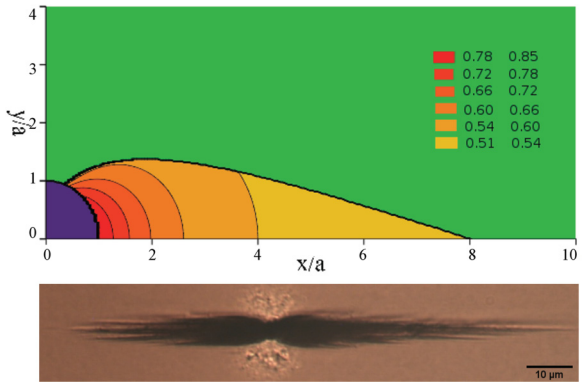

FIG. 17. (Color online) Concentration profile $\Phi(r,\theta)$ and shape of the nanoparticle cloud calculated by the pressure balance model [Eqs. (16)–(18)]. The initial volume fraction of nanoclusters is $\Phi_0 = 0.32\%$ (nanoparticle volume fraction $\phi_0 = 0.16\%$) and the external magnetic field intensity is $H_0 = 16$ kA/m. The color legend corresponds to the local nanocluster concentrations $\Phi(r,\theta)$ shown in absolute values. The nanoparticle cloud observed experimentally for the same parameters, ϕ_0 and H_0, is shown on the bottom of the figure.

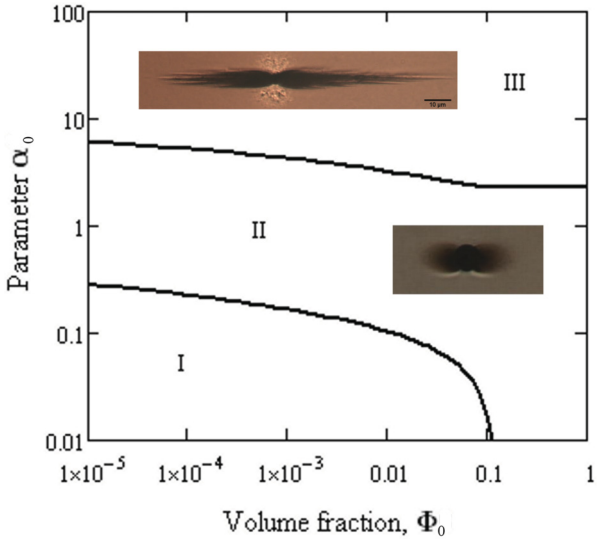

FIG. 18. (Color online) α_0-Φ_0 phase diagram showing the three regimes of nanoparticle and nanocluster accumulation around a spherical magnetic collector. In regime I, the nanocluster suspension is in the gas state at each point; in regime II, the suspension is in the gas state at infinity but is condensed into a liquid state in the vicinity of the microsphere; in regime III, a gas-liquid phase separation takes place in the whole volume of the nanocluster suspension.

experiments may be likely improved by exact computations of the magnetic field distribution inside and outside the clouds by a solution of the Maxwell equations with a free surface boundary condition [Eq. (17)] for the cloud interface.

Note that the iterative computations [Eqs. (10) and (16)–(18)] of the cloud surface and volume may be substantially simplified for relatively long clouds (extended along the z axis at a distance higher than 6–7 microsphere radii). In this case, we can neglect concentration variations along the cloud surface and consider that the concentration is approximately equal to the value $\Phi_L(\alpha_0)$ at infinity. So, the magnetic susceptibility χ is also supposed to be constant and is found using Eq. (2): $\chi = \text{const} \approx \chi(\Phi_L)$. The problem reduces to a single differential equation with respect to the cloud shape $R(\theta)$:

$$h^{*2} - h^2 = \chi \frac{(h_r - h_\theta R'/r)^2}{1 + (R'/r)^2}. \qquad (19)$$

Analysis shows that Eq. (19) gives only a few percent deviation for the cloud shape as compared to the full system of Eqs. (16)–(18).

V. CONCLUDING REMARKS

Both visualization experiments and the local thermodynamic equilibrium model have allowed us to reveal the extreme importance of the condensation phase transition on the sizes and shapes of nanoparticle clouds formed around a magnetized microsphere. Depending on the initial concentration of nanoparticles ϕ_0 (or nanoclusters, Φ_0) on their size and on the intensity of an external uniform magnetic field H_0, there can be three different regimes of nanoparticle accumulation around the microsphere, governed by the two dimensionless parameters $\alpha_0 = (\mu_0 H_0^2 V_c)/(2kT)$ and Φ_0. These regimes occupy certain areas in the phase diagram α_0-Φ_0, shown in Fig. 18. In the first regime, at relatively low parameters α_0, the nanoclusters do not condensate to a liquid state and their ensemble is in the gas state in all points around the microsphere. In this case, the nanocluster concentration around a microsphere varies smoothly with distance and is generally not very different from the initial concentration Φ_0, so the concentration field can be easily found with the help of the Boltzmann distribution. This regime, with negligible interactions between particles, was extensively studied previously (see, for instance, Ref. [14]) and is not considered in the present work. In the second regime, magnetic interactions between the nanoclusters become strong enough to induce a condensation phase transition near the microsphere, the nanocluster ensemble still being in the gas state far from the microsphere. In this regime, the nanoclusters are condensed into finite-sized "clouds" in an infinite volume suspension, and the cloud size increases progressively with both the initial concentration Φ_0 and the parameter α_0 (or, alternatively, with the external field intensity H_0 and the nanoparticle and nanocluster size). In the third regime, magnetic interactions become quite strong so that the condensation phase transition occurs not only in the vicinity of the microsphere but also at infinity from it, where highly concentrated and elongated droplets of nanoclusters appear. In an infinite volume suspension, the migration of these droplets towards the microsphere is an infinite process resulting in an infinite growth of the nanocluster clouds around the microsphere without reaching local thermodynamic equilibrium. In a real situation of a large but finite volume suspension, the migration of nanoclusters stops when the surrounding medium becomes sufficiently dilute and the thermodynamic equilibrium is established between the dilute (outside the cloud) and the concentrated (inside the cloud) phases.

We have proposed two different theoretical models to describe the concentration distribution and the nanoparticle cloud size and shape for the last two regimes. Both models consider phase transitions in the nanocluster ensemble in

slightly different ways. The local thermodynamic equilibrium approach was employed for the second regime, for which the gas-liquid phase equilibrium was calculated along the whole cloud interface. In this approach, we neglected the magnetic pressure jump on the gas-liquid interface such that the cloud surface corresponded to the surface of a constant magnetic field, at which the phase transition occurs. The pressure balance model was proposed for the case of finite volume nanocluster suspension in the third regime. We included the magnetic pressure jump into this model but neglected the presence of nanoclusters outside the cloud when calculating its shape. This second model captures reasonably well the highly elongated shapes of nanoparticle clouds. However, the quantitative agreement between theory and experiments remains rather poor. Nevertheless, the models allow us to predict the essential feature of the magnetic haloing phenomenon—the existence of the regimes of finite and infinite growth of nanoparticle clouds as well as a set of parameters (α_0,Φ_0) at which the transition between these regimes occur. Further improvements of the theory will be done by a combination of the thermodynamic and the pressure balance model as well as by the establishment of a more precise equation of state which would correctly account for chains or droplet formation in a bulk nanocluster suspension.

The results of the present paper could be useful for the further development of bimodal magnetorheological fluids used in smart hydraulic devices and of magnetic separation technologies used in bioanalysis and water purification systems.

ACKNOWLEDGMENTS

We would like to thank Dr. Sebastien Schaub and Yassin Bourras for assistance in experiments, as well as Professor Jacques Persello and Dr. Françoise Giulieri for helpful discussions. Financial support by projects Biomag (PACA, France), "Factories of the Future" (Grant No. 260073, DynExpert FP7), and CNRS ("exchange of scientists" project No. 23178) is gratefully acknowledged.

[1] V. Tohver, J. E. Smay, A. Braem, P. V. Braun, and J. A. Lewis, Proc. Natl. Acad. Sci. USA **98**, 8950 (2001).
[2] J. Liu and E. Luijten, Phys. Rev. Lett. **93**, 247802 (2004).
[3] S. A. Barr and E. Luijten, Langmuir **22**, 7152 (2006).
[4] S. Karanikas and A. A. Louis, Phys. Rev. Lett. **93**, 248303 (2004).
[5] E. N. Scheer and K. S. Schweizera, J. Chem. Phys. **128**, 164905 (2008).
[6] M. T. López-López, J. de Vicente, G. Bossis, F. González-Caballero, and J. D. G. Durán, J. Mater. Res. **20**, 874 (2005).
[7] J. L. Viota, F. González-Caballero, J. D. G. Durán, and A. V. Delgado, J. Colloid. Interface Sci. **309**, 135 (2007).
[8] M. T. López-López, P. Kuzhir, S. Lacis, G. Bossis, F. González-Caballero, and J. D. G. Durán, J. Phys.: Condens. Matter **18**, S2803 (2006).
[9] M. T. López-López, A. Yu. Zubarev, and G. Bossis, Soft Matter **6**, 4346 (2010).
[10] J. Svoboda, *Magnetic Techniques for the Treatment of Materials*, (Kluwer Academic, Dordrecht, 2004).
[11] M. Zborowski and J. J. Chalmers, *Magnetic Cell Separation* (Elsevier, Amsterdam, 2008).
[12] R. D. Ambashta and M. Sillanpää, J. Hazard. Mater. **180**, 38 (2010).
[13] R. Gerber, M. Takayasu, and F. Friedlaender, IEEE Trans. Magn. **19**, 2115 (1983).
[14] E. Blums, A. Cebers, and M. M. Mayorov, *Magnetic Fluids* (de Gruyters, Berlin, 1997).
[15] D. Fletcher, IEEE Trans. Magn. **27**, 3655 (1991).
[16] G. D. Moeser, K. A. Roach, W. H. Green, T. A. Hatton, and P. E. Laibinis, AIChE J. **50**, 2835 (2004).
[17] A. Ditsch, S. Lindenmann, P. E. Laibinis, D. I. C. Wang, and T. A. Hatton, Ind. Eng. Chem. Res. **44**, 6824 (2005).
[18] A. O. Tsebers, Magn. Gidrodin. **18**, 42 (1982) [Magnetohydrodynamics **18**, 137 (1982)].
[19] J. Liu, E. M. Lawrence, A. Wu, M. L. Ivey, G. A. Flores, K. Javier, J. Bibette, and J. Richard, Phys. Rev. Lett. **74**, 2828 (1995).
[20] Chin-Yih Hong, I. J. Jang, H. E. Horng, C. J. Hsu, Y. D. Yao, and H. C. Yang, J. Appl. Phys. **81**, 4275 (1997).
[21] D. Fletcher and M. R. Parker, J. Appl. Phys. **57**, 4289 (1985).
[22] O. Hovorka, B. Yellen, N. Dan, and G. Friedman, J. Appl. Phys. **97**, 10Q306 (2005).
[23] A. J. Kramer, J. J. M. Janssen, and J. A. A. J. Perenboom, IEEE Trans. Magn. **26**, 1858 (1990).
[24] E. Ya. Blum, A. Ya. Rimsha, and A. Yu. Chukhrov, Magn. Gidrodin. **23**, 28 (1987) [Magnetohydrodynamics **23**, 139 (1987)].
[25] Yu. A. Buyevich and A. O. Ivanov, Physica A **190**, 276 (1992).
[26] R. E. Rosensweig, *Ferrohydrodynamics* (Cambridge University Press, Cambridge, U.K., 1985).
[27] R. Massart, IEEE Trans. Magn. **17**, 1247 (1981).
[28] D. Bica, L. Vékás, M. V. Avdeev, O. Marinică, V. Socoliuc, M. Bălăsoiu, and V. M. Garamus, J. Magn. Magn. Mater. **311**, 17 (2007).
[29] W. B. Russell, D. A. Saville, and W. R. Schowalter, *Colloidal Dispersions* (Cambridge University Press, Cambridge, U.K., 1989).
[30] B. Faure, G. Salazar-Alvarez, and L. Bergström, Langmuir **27**, 8659 (2011).
[31] Q. Lan, Ch. Liu, F. Yang, Sh. Liu, J. Xu, and D. Sun, J. Colloid. Interface Sci. **310**, 260 (2007).
[32] R. Tadmor, R. E. Rosensweig, J. Frey, and J. Klein, Langmuir **16**, 9117 (2000).
[33] E. Tombácz, D. Bica, A. Hajdú, E. Illés, A. Majzik, and L. Vékás, J. Phys.: Condens. Matter **20**, 204103 (2008).
[34] A. Yu. Zubarev and L. Yu. Iskakova, Phys. Rev. E **65**, 061406 (2002).
[35] L. Yu. Iskakova, A. P. Romanchuk, and A. Yu. Zubarev, Physica A **366**, 18 (2006).
[36] A. Yu. Zubarev and L. Yu. Iskakova, Physica A **376**, 38 (2007).

[37] L. D. Landau and E. M. Lifshitz, *Statistical Physics*, Vol. 1 (Pergamon, Oxford, U.K., 1980), 3rd ed.
[38] N. F. Carnahan and K. E. Starling, J. Chem. Phys. **51**, 635 (1969).
[39] L. D. Landau, and E. M. Lifshitz, *Electrodynamics of Continuous Media* (Pergamon, New York, 1984).
[40] S. Berthier, *Optique des Milieux Composites* (Polytechnica, Paris, 1993).
[41] G. Banhegyi, Colloid Polym. Sci. **264**, 1030 (1986).
[42] H. Looyenga, Physica **31**, 401 (1965).
[43] R. B. Yang, S. D. Hsu, and C. K. Lin, J. Appl. Phys. **105**, 07A527 (2009).
[44] A. Yu. Zubarev and L. Yu. Iskakova, Phys. Rev. E **68**, 061203 (2003).
[45] L. D. Landau and E. M. Lifshitz, *A Course in Theoretical Physics—Fluid Mechanics*, Vol. 6 (Pergamon, New York, 1987).
[46] V. G. Bashtovoi, B. M. Berkovsky, and A. N. Vislovich, *Introduction to Thermomechanics of Magnetic Fluids* (Hemisphere, New York, 1988).